

The suppression of direct collapse black hole formation by soft X-ray irradiation

Kohei Inayoshi^{1*}, Takamitsu L. Tanaka^{2,3,4†}

¹*Department of Astronomy, Columbia University, 550 W. 120th Street, New York, NY 10027, USA*

²*Department of Physics and Astronomy, Stony Brook University, Stony Brook, NY 11794, USA*

³*Department of Physics, New York University, 4 Washington Place, New York, NY 10003, USA*

⁴*Max Planck Institute for Astrophysics, Karl-Schwarzschild-Str. 1, D-85741 Garching, Germany*

11 October 2018

ABSTRACT

The origin of supermassive black holes (SMBHs) in galactic nuclei is one of the major unsolved problems in astrophysics. One hypothesis is that they grew from $\gtrsim 10^5 M_\odot$ black holes that formed in the ‘direct collapse’ of massive gas clouds that have low concentrations of both metals and molecular hydrogen (H_2). Such clouds could form in the early ($z \gtrsim 10$) Universe if pre-galactic gas is irradiated by H_2 -photodissociating, far-ultraviolet (FUV) light from a nearby star-forming galaxy. In this work, we re-examine the critical FUV flux J_{crit} that is required to keep H_2 photodissociated and lead to direct collapse. We submit that the same galaxies that putatively supply the extraordinary FUV fluxes required for direct collapse should also produce copious amounts of soft X-rays, which work to offset H_2 photodissociation by increasing the ionization fraction and promoting H_2 formation. Accounting for this effect increases the value of J_{crit} by a factor of at least 3–10, depending on the brightness temperature of FUV radiation. This enhancement of J_{crit} suppresses the abundance of potential direct collapse sites at $z > 10$ by several orders of magnitude. Recent studies—without accounting for the soft X-rays from the FUV source galaxies—had already arrived at large values of J_{crit} that implied that direct collapse may occur too rarely to account for the observed abundance of high-redshift quasars. Our results suggest that J_{crit} should be even higher than previously estimated, and pose an additional challenge for the direct collapse scenario via strong FUV radiation to explain the high-redshift quasar population.

Key words: black hole physics, cosmology: theory, cosmology: dark ages, reionization, first stars, galaxies: formation, quasars: supermassive black holes

1 INTRODUCTION

Most nearby massive galaxies harbour a supermassive black hole (SMBH) in their nuclei. Empirical correlations between the masses of SMBHs and properties of their host galaxies suggest that SMBHs may play a key role in galaxy evolution, possibly during stages shining as luminous quasars (e.g. Magorrian et al. 1998; Ferrarese & Merritt 2000; Marconi & Hunt 2003; Hopkins et al. 2007; Kormendy & Ho 2013). Despite their apparent ubiquity and importance, when and how these cosmic behemoths formed remain poorly understood. Observations of luminous quasars at $z \gtrsim 6$ reveal that SMBHs with masses of $\gtrsim 10^9 M_\odot$ were already in place 900 Myr after the

Big Bang, and place strong constraints on possible formation scenarios (Fan et al. 2001; Fan 2006; Willott et al. 2010; Mortlock et al. 2011; Venemans et al. 2013; Bañados et al. 2014).

One possibility is that the earliest SMBHs grew from ‘seed’ $\sim 100 M_\odot$ BHs left behind by the first generation of stars (Population III or ‘Pop III’ stars) from $z \gtrsim 30$ via rapid gas accretion, aided by hierarchical BH mergers (Haiman & Loeb 2001; Madau & Rees 2001; Volonteri, Haardt & Madau 2003; Li et al. 2007; Tanaka, Perna & Haiman 2012; Tanaka, Li & Haiman 2013)¹. To form the $z > 6$ quasar SMBHs, these seeds must

¹ BH mergers play a secondary or minor role in BH growth. The gravitational recoil effect, while unlikely to prevent SMBH formation, suppresses the efficacy of mergers in assembling more massive BHs (Volonteri & Rees 2006; Tanaka & Haiman 2009).

* E-mail: inayoshi@astro.columbia.edu

† E-mail: takamitsu.tanaka@stonybrook.edu

have accreted gas at a mean rate comparable to the Eddington limit; a key uncertainty is whether Pop III remnant BHs could have maintained such rates despite negative radiative feedback in the shallow gravitational potentials of their host protogalaxies (Alvarez, Wise & Abel 2009; Milosavljević, Couch & Bromm 2009).

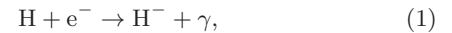
Alternatively, SMBHs could have originated as $\gtrsim 10^{5-6} M_{\odot}$ BHs that formed via the ‘direct collapse’ of gas clouds with low abundances of metals and molecular hydrogen (H_2) (e.g. Loeb & Rasio 1994; Oh & Haiman 2002; Bromm & Loeb 2003; Koushiappas, Bullock & Dekel 2004; Begelman, Volonteri & Rees 2006; Lodato & Natarajan 2006). Theoretically, direct collapse can occur in primordial gas clouds in massive dark-matter halos with virial temperatures of $\gtrsim 10^4$ K, if H_2 -line cooling is suppressed. The most widely studied H_2 -suppressing mechanism in this context is photodissociation by strong far-ultraviolet (FUV) radiation in the Lyman-Werner (LW) band (11.2 – 13.6 eV)². In such primordial gas without H_2 molecules, the gas loses thermal energy primarily via atomic hydrogen transitions ($Ly\alpha$, two-photon, and H^- free-bound emissions) and collapses while maintaining a temperature of ~ 8000 K (e.g., Omukai 2001). Recent numerical simulations have suggested that the gas can collapse monolithically avoiding the major-episode of fragmentation during the isothermal phase (Shang, Bryan & Haiman 2010; Regan & Haehnelt 2009a,b; Latif et al. 2013; Inayoshi, Omukai & Tasker 2014; Becerra et al. 2015).

After the collapse phase, a protostar with a mass of $\sim 1 M_{\odot}$ forms at the centre of the cloud and grows via rapid gas accretion at the rate of $\gtrsim 1 M_{\odot} \text{ yr}^{-1}$ (Inayoshi, Omukai & Tasker 2014). The protostar growing at such a high accretion rate evolves to a supermassive star within its lifetime ~ 1 Myr overcoming the radiative feedback and pulsation-driven mass loss (Hosokawa, Omukai & Yorke 2012; Inayoshi, Hosokawa & Omukai 2013; Hosokawa et al. 2013; Schleicher et al. 2013) and finally forms a massive seed BH by gravitational collapse due to general relativistic instability (Chandrasekhar 1964; Zeldovich & Novikov 1971; Shibata & Shapiro 2002). Compared to Pop III seed BHs, the products of direct collapse (‘direct collapse black holes,’ henceforth DCBH) require a somewhat lower (by ~ 10 to 20 per cent) mean accretion rate to grow to $\gtrsim 10^9 M_{\odot}$ by $z \sim 6 - 7$ (although the rate is still comparable to the Eddington limit; see e.g. Tanaka 2014 and references therein).

The most crucial question in the above scenario is how large the LW intensity must be to keep H_2 dissociated. This critical value, commonly called J_{crit} , has been discussed by many authors (Omukai 2001; Bromm & Loeb 2003; Shang, Bryan & Haiman 2010; Inayoshi & Omukai 2011; Wolcott-Green, Haiman & Bryan 2011; Latif et al. 2014). If the irradiating source has a thermal spectrum with a brightness temperature T_* , $J_{\text{crit}} \simeq \mathcal{O}(10)$ (in units of $10^{-21} \text{ erg s}^{-1} \text{ cm}^{-2} \text{ sr}^{-1} \text{ Hz}^{-1}$) for $T_* = 10^4$ K and $J_{\text{crit}} \simeq \mathcal{O}(10^3)$ for $T_* = 10^5$ K. For example, Sugimura, Omukai & Inoue (2014) recently obtained $J_{\text{crit}} \simeq 1400$ and found that this value does not change significantly between realistic UV

spectra of star-forming, low-metallicity galaxies. Several studies have estimated the probability of forming DCBHs via FUV fluxes $J_{\text{LW}} > J_{\text{crit}}$, using Monte Carlo calculations (Dijkstra et al. 2008; Dijkstra, Ferrara & Mesinger 2014, hereafter, DFM14) and semi-analytic methods coupled with N -body simulations (Agarwal et al. 2012). If $J_{\text{crit}} \gtrsim 10^3$, then the expected number density of DCBHs is comparable to or lower than that of SMBHs with $\gtrsim 10^9 M_{\odot}$ at $z \gtrsim 6$ (~ 1 comoving Gpc^{-3}). Recently, Latif et al. (2015) found that J_{crit} may be as large as $> 10^4$, further challenging the viability of the DCBH model to explain the observed SMBH population.

In this paper, we discuss the role of X-rays from the same star-forming galaxies that are the putative sources of H_2 -dissociating FUV radiation. X-rays can increase the hydrogen ionization fraction, promoting H_2 formation through the electron-catalyzed reactions



By working to *increase* the H_2 fraction, X-rays work against FUV photons and thus increase the effective value of J_{crit} —that is, we should generally expect

$$J_{\text{crit}}^{(\text{UV}+\text{X})} > J_{\text{crit}}^{(\text{UV only})} \quad (3)$$

if nearby galaxies irradiate putative DCBH formation sites with FUV *and* X-ray photons (Inayoshi & Omukai 2011). The above suggests that failing to account for the (H_2 -promoting) X-ray intensity that accompanies the (H_2 -dissociating) FUV intensity will generally result in an underestimate of J_{crit} .

That additional ionization sources in general (e.g. cosmic rays) can increase J_{crit} was made by Inayoshi & Omukai (2011). Recently, Latif et al. (2015) investigated the effect of $E \geq 2$ keV (hard) X-rays, which form a cosmic background because their mean free paths are too long to be absorbed locally. They found that the role of the X-rays become non-negligible at intensities $J_{X,21} > 0.01$, a value much higher than the expected background at $z > 10$. In this work, we invoke observational results from lower redshifts to argue that star-forming galaxies that supposedly irradiate putative DCBH formation sites with $J_{\text{LW},21} \gtrsim 2 \times 10^3$ should also supply a soft ($\lesssim 1$ keV) X-ray intensity $J_{X,21} \gtrsim 0.01$. We show that such intensities of soft local X-rays can raise J_{crit} , just as the previous works (Inayoshi & Omukai 2011; Latif et al. 2015) found for hard background X-rays.

For the most conservative assumption that high-redshift star-forming galaxies produce the same ratio of X-ray to FUV photons as local star-forming galaxies, accounting for X-ray ionizations increases J_{crit} by a factor of at least $\sim 3 - 10$ compared to previous work. This increase is highly sensitive to the actual X-ray to FUV flux ratio, and can be larger than an order of magnitude if early galaxies produce more X-rays relative to FUV photons. Following the semi-analytic methods of DFM14, we show that even a modest increase in J_{crit} reduces the abundance of DCBH formation sites by several orders of magnitude, further challenging the viability of the DCBH scenario.

We stress that this effect holds regardless of theoretical uncertainties in the calculation of the X-ray-uncorrected critical flux $J_{\text{crit}}^{(\text{UV only})}$. Whether $J_{\text{crit}}^{(\text{UV only})} \sim 10^3$ as suggested by one-zone calculations, or $\sim 10^4$ as suggested by

² For alternative mechanisms, see Inayoshi & Omukai (2012), Tanaka & Li (2014).

three-dimensional simulations, soft X-rays (~ 1 keV) from the FUV source galaxies will act to increase J_{crit} . In other words, the primary goal of this work is not to claim that J_{crit} may be too high to explain the observed SMBH abundance (as this has already been suggested by Latif et al. 2015 and others), but rather to demonstrate that it should be *higher* than found by previous studies that did not account for the soft X-ray output of the FUV source galaxies.

The rest of this paper is organised as follows. We describe in §2 our calculations of the critical LW intensity, in particular our treatment of X-ray ionization. In §3, we quantify the relation between LW and X-ray radiation from star-forming galaxies in the early Universe, and arrive at a relationship between the UV-only and X-ray-corrected values of J_{crit} ($J_{\text{crit}}^{\text{(UV only)}}$ and $J_{\text{crit}}^{\text{(UV+X)}}$, respectively). In §4, we apply these results to arrive at the X-ray-corrected probability that an atomic-cooling halo can form a DCBH. We estimate the number density of DCBHs as a function of J_{crit} and redshift. Finally, we present our conclusions in §5 and discuss the potential role of 21cm signatures and other observations in placing empirical constraints on FUV-aided DCBH formation.

2 EVALUATION OF J_{CRIT}

2.1 Thermal and chemical evolution

We consider the thermal evolution of primordial gas in a massive halo with a virial temperature of $\gtrsim 10^4$ K that is exposed to FUV radiation and X-rays from external sources. During the collapse of the self-gravitating cloud, its density profile approaches a self-similar form (Penston 1969; Larson 1969), consisting of a central core and an envelope with $\rho \propto r^{-2}$. We here adopt a one-zone model which approximates all the physical quantities to be uniform inside the central core, and solve for their temporal evolution (e.g., Omukai 2001).

The density of the central core increases on the free-fall timescale $t_{\text{ff}} = \sqrt{3\pi/32G\rho}$ as

$$\frac{d\rho}{dt} = \frac{\rho}{t_{\text{ff}}}. \quad (4)$$

The energy equation of the gas is given by

$$\frac{de}{dt} = -p \frac{d}{dt} \left(\frac{1}{\rho} \right) - \frac{\Lambda - \Gamma_{\text{X}}}{\rho}, \quad (5)$$

where e is the specific internal energy, p the gas pressure, Λ the cooling rate, and Γ_{X} the heating rate due to the external X-rays. We consider the radiative cooling by atomic and molecular hydrogen species, as well as the cooling/heating associated with chemical reactions. As the collapse proceeds and the gas grows denser, the intensity of external radiation that reaches the central core is reduced. We estimate the optical depth by assuming the size of the central core to be the half of the Jeans length λ_{J} . At the collapsing central core, the column density of the i -th species is given by

$$N_i = n(i) \frac{\lambda_{\text{J}}}{2}, \quad (6)$$

where $n(i)$ is the number density of the species.

We solve the primordial chemical reactions among the following 9 species: H, H₂, e⁻, H⁺, H₂⁺, H⁻, He, He⁺, and

Table 1. Photodissociation rates of H₂ and H⁻ (in cgs units) for thermal spectra with brightness temperature T_* .

| T_* (K) | 2×10^4 | 3×10^4 | 10^5 | (10^4) |
|---|-------------------|-----------------|--------|-------------------|
| $\kappa_{\text{H}_2} \times 10^{12}$ | 2.1 | 1.7 | 1.3 | 4.3 |
| $\kappa_{\text{H}^-} \times 10^{10}$ | 4.4 | 0.77 | 0.13 | 2000 |
| $k_{\text{H}^-}^{\text{pd}}/k_{\text{H}_2}^{\text{pd}}$ | 2.1×10^2 | 46 | 10 | 4.6×10^4 |

He⁺⁺. The chemical reactions we consider are the same as in Omukai (2001) but we have updated some reaction rate coefficients (Inayoshi, Omukai & Tasker 2014). We include the photoionization of H and He by X-rays.

The one-zone calculations start at $n = 0.1 \text{ cm}^{-3}$ and $T = 160$ K, which corresponds to the gas in a halo virializing at $z_{\text{vir}} \simeq 10$ (Omukai, Schneider & Haiman 2008). We set the initial abundances of electrons, H₂, and He to $x_e = 10^{-4}$, $x_{\text{H}_2} = 10^{-6}$, and $x_{\text{He}} = 0.08$, respectively. These initial conditions are the same as in Inayoshi & Omukai (2011).

2.2 External FUV and X-ray radiation

We now discuss our treatment of FUV and X-ray radiation, and in particular how X-rays affect the effective value of J_{crit} . Below, we use the symbol $J_{\text{crit},0} \equiv J_{\text{crit}}^{\text{(UV only)}}$ to denote the value of J_{crit} calculated without considering the effects of X-ray ionizations.

2.2.1 FUV radiation

We assume the FUV radiation to have a diluted thermal spectrum, $J_{\text{LW}}(\nu) \propto B_\nu(T_*)$, and consider brightness temperatures of $T_* = 2 \times 10^4$, 3×10^4 and 10^5 K. These values of T_* correspond to realistic spectra of Pop II/III star-forming galaxies, the FUV sources near DCBH forming halos (see §3.1.2). We normalise the intensity of the FUV radiation at the Lyman limit ($\nu_{\text{L}} = 13.6$ eV), and write this in conventional units: $J_{\text{LW},21} = J_{\text{LW}}(\nu_{\text{L}})/(10^{-21} \text{ erg s}^{-1} \text{ cm}^{-2} \text{ sr}^{-1} \text{ Hz}^{-1})$. For the thermal spectra we adopt, the rate coefficients for photodissociation of H₂ and H⁻ are given by $k_{\text{H}_2}^{\text{pd}} \equiv \kappa_{\text{H}_2} J_{\text{LW},21}$ and $k_{\text{H}^-}^{\text{pd}} \equiv \kappa_{\text{H}^-} J_{\text{LW},21}$, respectively. The values of $\kappa_{\text{H}_2(\text{H}^-)}$ for each T_* are listed in Table 1. We have also included the case $T_* = 10^4$ K for reference. We also consider the H₂ self-shielding effect against external FUV radiation (Wolcott-Green, Haiman & Bryan 2011).

2.2.2 X-rays

We assume that the X-ray mean intensity can be represented by a power-law spectrum,

$$J_{\text{X}}(\nu) = J_{\text{X},21} \times 10^{-21} \left(\frac{\nu}{\nu_0} \right)^{-\alpha} \text{ erg s}^{-1} \text{ cm}^{-2} \text{ sr}^{-1} \text{ Hz}^{-1}, \quad (7)$$

where $h\nu_0 = 1$ keV and $\alpha = 1.8$ (e.g. Swartz et al. 2004). The ionization rates of H and He by direct X-ray photons

are given by

$$\zeta_{X,p}^i = \int_{\nu_{\min}}^{\nu_{\max}} \frac{4\pi J_X(\nu)}{h\nu} e^{-\tau_\nu} \sigma_i(\nu) d\nu \quad (i = \text{H, He}), \quad (8)$$

$$\tau_\nu = N_{\text{H}}\sigma_{\text{H}}(\nu) + N_{\text{He}}\sigma_{\text{He}}(\nu), \quad (9)$$

where $\sigma_{\text{H}}(\nu)$ and $\sigma_{\text{He}}(\nu)$ are the cross sections of H and He to the ionizing photons (Verner et al. 1996; Yan, Sadeghpour & Dalgarno 1998, respectively)³ and N_{H} and N_{He} are the column densities of those species. Since the emitted electrons have large kinetic energy, they can ionise the surrounding gas (secondary ionization). We also estimate the secondary ionization and X-ray heating rates using the formulae in Shull & van Steenberg (1985), which are valid for X-ray photons with energies $\gg 0.1$ keV.

In this calculation, we set the maximum energy of the X-rays to $h\nu_{\max} = 10$ keV. The following results do not depend on the choice of ν_{\max} as long as $h\nu_{\max} \geq 10$ keV. The X-ray minimum energy is the more important quantity. The comoving mean free path of a X-ray photon with $h\nu$ can be written as

$$\lambda_X \simeq 9.1 \bar{x}_{\text{H}}^{-1} \left(\frac{1+z}{11} \right)^{-2} \left(\frac{h\nu}{0.3 \text{ keV}} \right)^3 \text{ cMpc}, \quad (10)$$

where \bar{x}_{H} is the mean neutral fraction (Furlanetto, Oh & Briggs 2006). From the condition that λ_X is longer than the Hubble horizon, hard X-ray photons with $\gtrsim 2$ keV can build up a cosmic X-ray background before $z \sim 10$ (e.g. Ricotti & Ostriker 2004; Tanaka, Perna & Haiman 2012). On the other hand, the FUV sources required to form DCBHs are star-forming galaxies close to the DCBH forming halo. The physical separation is typically ~ 10 kpc (Dijkstra et al. 2008), which is much shorter than $\lambda_X/(1+z) \sim 800$ kpc. We therefore argue that soft X-rays with energies $h\nu < 2$ keV, if produced by the FUV sources, must irradiate potential DCBH formation sites. Given the uncertainty in the X-ray emission properties of the earliest star-forming galaxies, we consider minimum X-ray energies of $h\nu_{\min} = 0.5$ and 1 keV. For comparison to previous works, we also consider the case $h\nu_{\min} = 2$ keV.

2.3 X-ray enhancement of the critical LW flux

In Fig. 1, we present the ratio of $J_{\text{crit}}/J_{\text{crit},0}$ (FUV+X to FUV only) as a function of the X-ray intensity $J_{X,21}$. The solid curves show cases with $h\nu_{\min} \leq 1$ keV and $T_* = 2 \times 10^4$ K (blue), 3×10^4 K (green), and 10^5 K (red) from bottom to top. The dashed blue curve shows the case $h\nu_{\min} = 2$ keV and $T_* = 2 \times 10^4$ K, for comparison with a previous study (Latif et al. 2015, see below).

Let us first discuss the case $h\nu_{\min} = 1$ keV. For weak X-ray intensities, the value of $J_{\text{crit}}/J_{\text{crit},0}$ converges to a constant value of ≈ 1 . The critical LW intensity increases with the X-ray intensity at $J_{X,21} \gtrsim 10^{-3}$ for all cases of

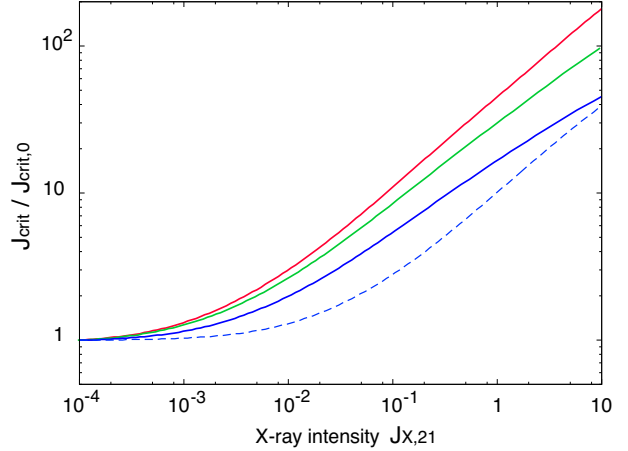


Figure 1. The ratio $J_{\text{crit}}/J_{\text{crit},0}$, the relative increase in the requisite FUV intensity to photodissociate H_2 molecules inside an atomic-cooling halo, when X-rays are added to the radiating spectrum. The solid lines show the cases for $h\nu_{\min} = 1$ keV; from bottom to top: $T_* = 2 \times 10^4$ K (blue curve), 3×10^4 K (green) and 10^5 K (red). The results for $h\nu_{\min} = 0.5$ keV are nearly identical to those for $h\nu_{\min} = 1$ keV and we do not show them here. The dashed line shows the case of $h\nu_{\min} = 2$ keV and $T_* = 2 \times 10^4$ K, for comparison with the previous study. A colour version of this figure is available in the online version.

T_* . This is because the electron fraction rises through X-ray ionization and thus the H_2 formation rate through the reactions in equation (1) and (2) increases (We show the evolution of the electron fraction and discuss the effect of X-ray ionization on its behavior in the Appendix.). For all cases considered here, the functional form of J_{crit} can be fitted as $J_{\text{crit}}/J_{\text{crit},0} = (1 + J_{X,21}/a)^b$, where $(J_{\text{crit},0}, a, b) = (1.7 \times 10^3, 3.4 \times 10^{-3}, 0.50)$, $(2.4 \times 10^3, 2.2 \times 10^{-3}, 0.56)$ and $(3.1 \times 10^3, 2.1 \times 10^{-3}, 0.62)$ for $T_* = 2 \times 10^4$, 3×10^4 and 10^5 K, respectively⁴

Next, we address the dependence of the critical FUV intensity on the X-ray intensity and the FUV spectrum. As many authors have shown (e.g., Omukai 2001; Inayoshi & Omukai 2011), the value of $J_{\text{crit},0}$ for hard spectra ($T_* \gtrsim 2 \times 10^4$ K) is well-approximated by a functional form $f(T_*)x_e$, because H^- photodissociation is negligible for $J_{\text{crit},0}$ in such harder spectra (see Inayoshi & Omukai 2011, for details). That is, the value of $J_{\text{crit},0}$ scales linearly with the electron fraction and the normalization depends on the FUV spectrum. The primary role of the X-rays is to raise J_{crit} by increasing the equilibrium value of x_e . For simplicity, if we assume that the X-ray ionization and recombination are balanced in the collapsing cloud, the electron fraction is expressed as $x_e \propto J_{X,21}^{1/2}$. This approximation is valid for $n_{\text{H}} \lesssim 10^4 \text{ cm}^{-3}$ and explains why the power-law index $b \simeq 0.5$ for the fitting form described in the previous paragraph. Thus, $J_{\text{crit}}/J_{\text{crit},0}$ can be approximated by the ratio of the values of x_e obtained with and without X-

³ Previously, Inayoshi & Omukai (2011) adopted the cross sections by Rybicki & Lightman (1979) (for H) and Osterbrock (1989) (for He). These works overestimate the cross sections at X-ray energies. In this work we adopt the more recent cross sections referenced above.

⁴ If we normalise the FUV intensity at the average energy of the LW band (12.4 eV) instead of $\nu_{\text{L}} = 13.6$ eV, the values of $J_{\text{crit},0}$ become a constant ($\simeq 2.7 \times 10^3$) for all cases of $2 \times 10^4 \leq T_* \leq 10^5$ K. This dependence on T_* agrees with previous work (Sugimura, Omukai & Inoue 2014).

ray ionizations—that is, it depends most sensitively on the X-ray intensity, and depends weakly on the choice of FUV spectrum as long as H^- photodissociation is negligible. We provide extended descriptions of the above relationships in the Appendix, and direct readers there for additional details.

The values of $J_{\text{crit}}/J_{\text{crit},0}$ for $T_* = 3 \times 10^4$ K are indeed close to those for $T_* = 10^5$ K. However, for a high value of J_{crit} , the *indirect* H_2 dissociation through the H^- photodissociation begins to work against H_2 formation by the reaction in equation (2)—i.e. $\kappa_{\text{H}^-} J_{\text{crit}} > k_2 n_{\text{H}_2}^{\text{crit}} \simeq 1.1 \times 10^{-6}$ at $T \simeq 8000$ K, where k_2 is the rate coefficient of the reaction (2) and $n_{\text{H}_2}^{\text{crit}}$ is the critical density of H_2 . The above condition is written as $J_{\text{crit}}/J_{\text{crit},0} > 1.5, 6.0,$ and 27 for $T_* = 2 \times 10^4$ K, 3×10^4 K and 10^5 K, respectively. Therefore, for larger J_{crit} , the increase of $J_{\text{crit}}/J_{\text{crit},0}$ becomes slightly smaller. In Fig. 1, this can be seen in the decrease in the slope of this ratio at large $J_{\text{X},21}$ for the $T_* = 2 \times 10^4$ K case. However, we note that this effect is smaller than many other uncertainties in evaluating J_{crit} (see §3.2).

We study the dependence of the critical LW intensity J_{crit} on the choice of $h\nu_{\text{min}}$. In the case of $h\nu_{\text{min}} = 2$ keV, the minimum X-ray intensity for increasing J_{crit} is larger by one order of magnitude than that for our fiducial model ($h\nu_{\text{min}} = 1$ keV). This is because the cross sections of H and He against photons with energies $\gtrsim 2$ keV are small and thus the X-ray ionization is also less important. For this case, the fitted parameters are given by $(J_{\text{crit},0}, a, b) = (1.7 \times 10^3, 2.2 \times 10^{-2}, 0.6)$. The curve for $h\nu_{\text{min}} = 2$ keV shifts rightwards by approximately one order of magnitude compared to that for $h\nu_{\text{min}} = 1$ keV.

Recently, Latif et al. (2015) studied the effect of X-rays on DCBH formation by considering hard X-rays ($h\nu_{\text{min}} = 2$ keV) that comprise the X-ray background radiation. In their result, the critical FUV intensity begins to increase at $J_{\text{X},21} \gtrsim 10^{-2}$ and boosts by a factor of ≈ 2 at $J_{\text{X},21} \simeq 10^{-1}$. This is consistent with our findings, represented by the blue dashed curve in Fig. 1. Note that this result is robust to changes in T_* , as explained above. As seen the dashed line (blue) in Fig. 1, our result is $J_{\text{crit}}/J_{\text{crit},0} \approx 2.5$ for $J_{\text{X},21} \simeq 10^{-1}$, which is consistent with their three-dimensional simulation. A minimum energy of $h\nu_{\text{min}} = 2$ keV is a reasonable assumption for the cosmic X-ray background, as soft X-rays with 0.5 (1) keV would be absorbed at separations of ~ 40 (300) Mpc in the intergalactic medium. However, the *nearby* halos that putatively enable DCBH formation through large FUV fluxes should also irradiate their immediate environments with soft (~ 1 keV) X-rays. *We emphasize the key point that soft X-rays are far more effective at promoting H_2 formation through electron-catalyzed reactions.*

On the other hand, the result for $h\nu_{\text{min}} = 0.5$ keV does not change from our fiducial model ($h\nu_{\text{min}} = 1$ keV). The value of J_{crit} is determined by the electron fraction at $n_{\text{H}} \simeq 10^3 \text{ cm}^{-3}$ and $T \simeq 8000$ K (Inayoshi & Omukai 2011). The photons with $h\nu_{\text{min}} \lesssim 1$ keV can ionise the gas easily and thus are absorbed at $n_{\text{H}} < 10^3 \text{ cm}^{-3}$. We conclude that the value of J_{crit} is sensitive to the intensity of X-ray photons at $\simeq 1$ keV but not to that of softer X-rays at energies $\lesssim 1$ keV.

Here, we have assumed a simple power-law spectrum with $J_{\text{X}}(\nu) \propto \nu^{-1.8}$. However, the spectral energy distributions of observed high-mass X-ray binaries (HMXBs) are more complex (e.g., Gierlinski et al. 1997; Gierliński et al.

1999; Swartz et al. 2004). The spectral shapes are characterised by a power-law with $\alpha \approx 1.6 - 1.8$ (low-hard state) and by a bright thermal component with a peak temperature of ~ 0.5 keV having a soft power-law tail with $\alpha \gtrsim 2.0$ (high-soft state). We note that the resulting value of $J_{\text{crit}}/J_{\text{crit},0}$ for $h\nu_{\text{min}} \leq 1$ keV depends very weakly on the choice of the X-ray power-law index in the range of $1.6 \lesssim \alpha \lesssim 2.0$ because ionization by soft X-rays (~ 1 keV) increases J_{crit} significantly. The X-ray spectra of HMXBs in high- z galaxies could have an excess due to the thermal emissions from the power-law component at $\sim 1 - 10$ keV (Fragos et al. 2013b). We note that the value of J_{crit} begins to increase for X-ray intensities as small as $J_{\text{X},21} \sim 10^{-3}$ in a case with thermal soft X-ray components.

3 LW AND X-RAY SOURCES IN THE EARLY UNIVERSE

Having laid out above the general effect of X-ray fluxes on the quantity J_{crit} , we now turn to the discussion of X-ray and LW sources in the $z \gtrsim 10$ Universe.

3.1 FUV and X-ray intensities

3.1.1 X-ray flux

We first estimate the X-ray intensities from the star-forming galaxies in the $z \sim 20 - 10$ Universe. According to the most recent cosmological simulations, Pop III stars could be born as massive stars with $\sim 10 - 100 M_{\odot}$ (e.g., Hosokawa et al. 2011; Stacy, Greif & Bromm 2012; Hirano et al. 2014). Moreover, the efficiency of forming binary systems could be as high as $\sim 50\%$ (e.g., Stacy & Bromm 2013; Susa, Hasegawa & Tominaga 2014). Thus, we can consider HMXBs as X-ray sources in the early Universe (e.g. Power et al. 2009; Mirabel et al. 2011)⁵.

From observations of local starburst galaxies, we can obtain a good correlation between the X-ray luminosities and their star formation rate (SFR). The X-ray emission is dominated by HMXBs, which is considered to be good tracers of the SFR because of their short lifetime. The bolometric X-ray luminosity (2–10 keV) is given by

$$L_{2-10\text{keV}} \simeq 6.7 \times 10^{39} \left(\frac{\text{SFR}}{M_{\odot} \text{ yr}^{-1}} \right) \text{ erg s}^{-1}, \quad (11)$$

(e.g. Grimm, Gilfanov & Sunyaev 2003; Glover & Brand 2003). Many observations in various X-ray bands also have suggested the same L_{X} -SFR relation within a factor of 2–3 (e.g., Grimm, Gilfanov & Sunyaev 2003; Lehmer et al. 2010; Mineo, Gilfanov & Sunyaev 2012). Furthermore, the dispersion of L_{X}/SFR is at most ~ 0.4 dex (Mineo, Gilfanov & Sunyaev 2012). Assuming a simple power-law spectrum with $L_{\text{X}}(\nu) \propto \nu^{-\alpha}$ (see equation 7), we can estimate the X-ray flux at 1 keV (in units of

⁵ Another candidate is a supernova remnant where accelerated electrons emit X-ray photons. However, the X-ray from supernova remnants could be subdominant because of their transient nature (Oh 2001; Furlanetto 2006; Mirabel et al. 2011).

10^{-21} erg s $^{-1}$ cm $^{-2}$ sr $^{-1}$ Hz $^{-1}$) as

$$J_{X,21} = \left\{ \begin{array}{c} 0.68 \\ 0.89 \\ 1.2 \end{array} \right\} \times 4 \times 10^{-4} \left(\frac{\text{SFR}}{\text{M}_{\odot} \text{ yr}^{-1}} \right) \left(\frac{d}{10 \text{ kpc}} \right)^{-2}, \quad (12)$$

where the three values in brackets correspond to cases for $\alpha = 1.6, 1.8,$ and 2.0 (from top to bottom).

Several studies have investigated the redshift evolution of the L_X -SFR relation using empirical data. The linear relation observed in local star-forming galaxies ($z = 0$) does not change significantly up to $z \lesssim 2$ (Grimm, Gilfanov & Sunyaev 2003; Lehmer et al. 2008; Mineo et al. 2014). The Chandra Deep Field-South suggests that the ratio increase as $\propto (1+z)$ out to $z \sim 4$ (Basu-Zych et al. 2013). Furthermore, the existence of the unresolved soft X-ray background places a constraint on its evolution at higher redshifts: $d \log(L_X/\text{SFR})/d \log(1+z) \leq 1.3$ (Dijkstra et al. 2012).

As noted above, the latest simulations suggest that Pop III stars tend to form with large ($> 10 \text{ M}_{\odot}$) masses in binary or multiple systems. Thus, we expect more X-ray binaries in the high- z Universe than in the local galaxies. Although the properties of Pop III binaries remain highly uncertain, Hummel et al. (2014) estimate that they produced an X-ray background intensity $J_{X,21} \sim 0.03$ at $z \sim 20$. This value is a few hundred times larger than the L_X/SFR of low- z galaxies. Similarly, population synthesis models of Fragos et al. (2013a,b) predict that L_X/SFR at $z \sim 10$ is higher than the local value by an order of magnitude.

To keep our results and discussions conservative, we here adopt the X-ray intensity using the L_X -SFR relation obtained from observations of low- z galaxies (instead of theoretical extrapolations of the ratio to higher redshifts). We define the dimensionless number in curly brackets in equation (12) as $f_X \equiv J_{X,21}/(4 \times 10^{-4}) \simeq 1$ and treat it as a parameter set fiducially to unity (note that f_X has an empirical dispersion of 0.4 dex in low- z galaxies; Mineo, Gilfanov & Sunyaev 2012). As we describe above, both observations and theoretical works suggest $f_X \gtrsim 1-10$. We note that our fiducial model is in close agreement with Mesinger, Ferrara & Spiegel (2013), who used/found $f_X \approx 1$ based on the number of X-ray photons per stellar baryon $N_X \approx 0.2$ and the fraction of baryons converted into stars $f_* \approx 0.1$ ⁶.

3.1.2 FUV radiation

Next, we estimate the LW intensities from star-forming galaxies consisting of Pop II ($Z = 10^{-3}$) and Pop III stars ($Z = 0$). We adopt the Salpeter initial mass function ($1 \leq M_* \leq 100 \text{ M}_{\odot}$). The number flux of LW photons is estimated as $Q_{\text{LW}} = 5.25 (3.72) \times 10^{53} \text{ s}^{-1}$ ($\text{SFR}/\text{M}_{\odot} \text{ yr}^{-1}$) for the Pop II (III) case, assuming constant star formation (Schaerer 2003). To estimate the mean intensity at 13.6 eV, we here consider two types of spectral models of star-forming

⁶ While we choose $f_X = 1$ as our fiducial model, the fiducial models of most previous theoretical studies (e.g. Furlanetto 2006; Pritchard & Furlanetto 2007) correspond to $f_X \approx 4-5$ in our notation.

Table 2. The ratio of the photodissociation rates of H $_2$ and H $^-$ for Pop II galaxies.

| constant star formation: 100 Myr ^a | | | |
|---|-----------------|--------------------|--------------------|
| $Z(Z_{\odot})$ | 0 | 5×10^{-4} | 2×10^{-2} |
| $k_{\text{H}^-}^{\text{pd}}/k_{\text{H}_2}^{\text{pd}}$ | 4.2×10 | 3.9×10 | 5.4×10 |
| instantaneous starburst : 100 Myr ^b | | | |
| $Z(Z_{\odot})$ | 0 | 5×10^{-4} | 2×10^{-2} |
| $k_{\text{H}^-}^{\text{pd}}/k_{\text{H}_2}^{\text{pd}}$ | 3.8×10 | 5.6×10 | 2.2×10^2 |

^aThe duration of star formation.

^bThe time since the starburst.

References: Inoue (2011); Sugimura, Omukai & Inoue (2014).

galaxies: (i) a thermal spectrum with the effective temperature of $\geq 2 \times 10^4$ K and (ii) a flat spectrum ($\propto \nu^{0-0.5}$ at $1 \lesssim h\nu \leq 13.6$ eV), which may be expected because of the superposition of radiation from low-mass and massive stars (Inoue 2011). We find

$$J_{\text{LW},21} = \left\{ \begin{array}{c} 0.85 \\ 1.1 \\ 1.0 \\ 1.3 \end{array} \right\} \times 90 \left(\frac{\text{SFR}}{\text{M}_{\odot} \text{ yr}^{-1}} \right) \left(\frac{d}{10 \text{ kpc}} \right)^{-2}, \quad (13)$$

where the first three values in brackets correspond to cases for thermal spectra with $T_* = 2 \times 10^4, 3 \times 10^4$ and 10^5 K (with the third value corresponding to the PopIII case), and the fourth value to the flat spectrum. The actual effective temperatures of Pop II galaxies are hotter than 10^4 K (Inoue 2011). The ratio of $k_{\text{H}^-}^{\text{pd}}/k_{\text{H}_2}^{\text{pd}}$, which is a good indicator of $J_{\text{crit},0}$ (Sugimura, Omukai & Inoue 2014), decreases for higher T_* . We summarize the the values of these ratios for spectral models of Pop II galaxies in Table 2. For most cases (except for the instantaneous starburst model with $2 \times 10^{-2} Z_{\odot}$), the ratio is smaller than 60. Thus, as far as the critical FUV intensity is concerned, these spectral models are closest to the case of a thermal spectrum with $T_* \simeq 3 \times 10^4$ K (see Table 1). We will call the dimensionless factor in the curly brackets as $f_{\text{LW}} (\simeq 1)$.

3.1.3 Relation between X-rays and FUV radiation

Combining the expressions for J_X and J_{LW} above, we obtain

$$\frac{J_{X,21}}{J_{\text{LW},21}} \simeq 4.4 \times 10^{-6} \left(\frac{f_X}{f_{\text{LW}}} \right). \quad (14)$$

Above, $f_X \gtrsim 1-10$ is the normalization of the X-ray intensity with respect to low- z star-forming galaxies (§3.1.1, eq. 12), and $f_{\text{LW}} \simeq 1$ is the dependence of the J_{LW} normalization on the galaxy FUV spectrum (§3.1.2, eq. 13). For example, if a star-forming galaxy has the same ratio of X-rays to FUV photons as the value typically found in lower-redshift galaxies ($f_X/f_{\text{LW}} = 1$) and irradiates a neighboring halo at an FUV intensity $J_{\text{LW},21} \gtrsim 2 \times 10^3$, then it will simultaneously expose it to a soft X-ray intensity $J_{X,21} \gtrsim 0.01$. In what follows, we consider a wide range $0.1 \leq f_X/f_{\text{LW}} \leq 10$ in order to present a conservative discussion.

Table 3. The enhancement factor of the critical FUV intensity ($J_{\text{crit}}/J_{\text{crit},0}$) at the intersection points between solid curves and dashed lines in Fig. 2. The first three columns are the cases for $h\nu_{\text{min}} = 1$ keV and the fourth is for $h\nu_{\text{min}} = 2$ keV.

| T_* (K) | 2×10^4 | 3×10^4 | 10^5 | $(2 \times 10^4; 2 \text{ keV})$ |
|-------------------------|-----------------|-----------------|--------|----------------------------------|
| $f_X/f_{\text{LW}} = 1$ | 2.5 | 7.0 | 22 | 1.3 |
| $f_X/f_{\text{LW}} = 3$ | 6.5 | 26 | 120 | 1.9 |

3.2 Critical LW intensity

In Fig. 2, we show how the critical LW intensity J_{crit} increases when accounting for X-ray ionizations. This figure shows the relationship between the X-ray-corrected value (J_{crit}) and the value calculated assuming a UV-only spectrum ($J_{\text{crit},0}$). As described above, the critical LW intensity J_{crit} increases in the presence of an X-ray flux. For the purposes of computing J_{crit} , the spectra of Pop II galaxies are well described by a thermal spectrum with $T_* \simeq 3 \times 10^4$ K (see §3.1.2). In what follows, we consider this case as our fiducial model. For $h\nu_{\text{min}} = 1$ keV (solid curves), the X-ray-corrected value can be fit by the following simple formula (§2):

$$J_{\text{crit}} = J_{\text{crit},0} \left(1 + \frac{J_{X,21}}{2.2 \times 10^{-3}} \right)^{0.56}. \quad (15)$$

where $J_{\text{crit},0}$ is the value calculated without considering X-ray ionizations at all. Using equation (14), the actual critical LW intensity J_{crit} can be written in terms of the original critical LW intensity (i.e., no X-ray flux) as

$$J_{\text{crit}} \simeq 1.8 \times 10^4 \left(\frac{J_{\text{crit},0}}{2.4 \times 10^3} \right)^{2.3} \left(\frac{f_X}{f_{\text{LW}}} \right)^{1.3}, \quad (16)$$

which corresponds to an intersection of the solid curve (green) and thick dotted line in Fig. 2. This equation is approximately valid for $f_X/f_{\text{LW}} \gtrsim 0.2$ ($J_{\text{crit},0}/2.4 \times 10^3$) $^{-1}$; at these values, X-ray ionization suppresses DCBH formation by raising the value of the critical flux J_{crit} necessary to keep H_2 photodissociated.

In Table. 3, we summary the values of $J_{\text{crit}}/J_{\text{crit},0}$ at the intersection points between solid curves and dashed lines in Fig. 2 for various cases. If $f_X/f_{\text{LW}} \sim 1$, and if the X-ray-uncorrected value $J_{\text{crit},0} \gtrsim 2 \times 10^3$, then soft X-rays would increase J_{crit} by a factor of $\sim 3 - 10$. As we will discuss in the next section, even such a modest increase in J_{crit} is expected to decrease the abundance of potential DCBH sites by several orders of magnitude (DFM14). However, we have earlier described calculations showing that $f_{\text{LW}} \sim 1$ for several irradiation spectra, and $f_X \sim 1 - 10$ for $z \gtrsim 10$ galaxies. Taken together, those results suggest $f_X/f_{\text{LW}} > 1$ at redshifts relevant for direct collapse, in which case the suppression of DCBH sites is much more severe than in our fiducial, conservative case $f_X/f_{\text{LW}} = 1$.

Equation (16) shows that J_{crit} is sensitive to the value of $J_{\text{crit},0}$. The higher the value of $J_{\text{crit},0}$ (e.g. higher T_*), the critical LW flux evaluated without taking into account X-ray ionizations, the higher the value of the effective value J_{crit} . The relative enhancement is roughly proportional to the FUV intensity itself. In addition, we find that soft X-rays are suitable for increasing J_{crit} more than hard X-rays because f_X is effectively smaller by one order of magnitude

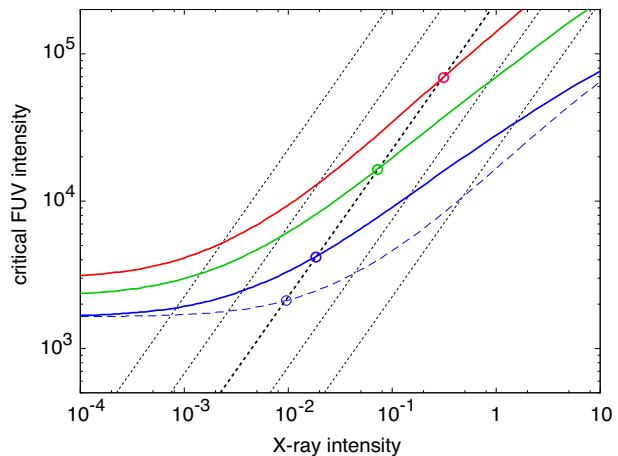


Figure 2. J_{crit} vs. J_X . The critical LW intensity J_{crit} as a function of the X-ray intensity $J_{X,21}$ for $T_* = 2 \times 10^4$, 3×10^4 and 10^5 K from bottom to top (solid curves; $h\nu_{\text{min}} = 1$ keV) and for $T_* = 2 \times 10^4$ K (dashed curve; $h\nu_{\text{min}} = 2$ keV). Dotted lines show the relation between the LW and X-ray intensities given by equation (14): fiducial model ($f_X/f_{\text{LW}} = 1$; thick dotted) and the cases for $f_X/f_{\text{LW}} = 1/10$, $1/3$, 3 and 10 (thin dotted). A colour version of this figure is available in the online version.

Table 4. Summary of the critical LW intensity $J_{\text{crit},0}$

| authors | $J_{\text{crit},0}$ | T_* (K) | method |
|---------|---------------------|-------------------|----------|
| SBH10 | 39 | 10^4 | one-zone |
| | 30 – 300 | 10^4 | 3D |
| IO11 | 20 | 10^4 | one-zone |
| L14 | 400 – 1500 | 10^4 | 3D |
| SOI14 | 25 | 10^4 | one-zone |
| SOI14 | $\gtrsim 1400$ | $> 2 \times 10^4$ | one-zone |
| SBH10 | 1.2×10^4 | 10^5 | one-zone |
| | $10^4 - 10^5$ | 10^5 | 3D |
| IO11 | 1.6×10^4 | 10^5 | one-zone |
| WHB11 | $2 - 4 \times 10^3$ | 10^5 | 3D |

References: Shang, Bryan & Haiman (2010) (SBH10); Inayoshi & Omukai (2011) (IO11); Wolcott-Green, Haiman & Bryan (2011) (WHB11); Latif et al. (2014) (L14); Sugimura, Omukai & Inoue (2014) (SOI14).

for the case of hard X-rays. For $h\nu_{\text{min}} = 2$ keV (dashed line in Fig. 2), the X-ray-corrected value is almost the same as the original value.

The critical LW intensity evaluated without consideration of external ionizations, $J_{\text{crit},0}$, has been investigated using a one-zone model (e.g., Omukai 2001; Inayoshi & Omukai 2011) and three-dimensional numerical simulations (e.g., Bromm & Loeb 2003; Shang, Bryan & Haiman 2010; Wolcott-Green, Haiman & Bryan 2011; Latif et al. 2014). We summarize the results of these previous studies in Table 4. For a soft spectrum with $T_* = 10^4$ K, the values of $J_{\text{crit},0}$ are $20 - 40$ (one-zone models) and $30 - 10^3$ (3D simulations). For harder spectra with $T_* > 2 \times 10^4$ K, the values of $J_{\text{crit},0}$ are $\gtrsim 10^3$ (one-zone models) and $\sim 10^4$ (3D simulations). Sugimura, Omukai & Inoue (2014) found

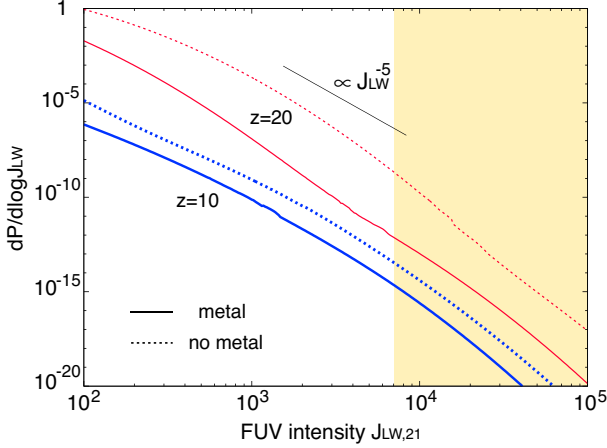


Figure 3. The probability distribution function (PDF) of atomic-cooling halos (mass M_{ac}) being exposed to an FUV intensity J_{LW} by a neighbouring star-forming galaxy. The thick (blue) lines show the cases at $z = 10$, and the thin (red) lines show the cases at $z = 20$. The solid and dashed lines show the cases with and without metal enrichment, respectively, by galactic outflows from the FUV source. The PDF is well-characterised by a power law with index ≈ 5 in the range $J_{\text{LW},21} \sim 10^3 - 10^4$. The shaded region shows the required J_{LW} intensity for forming DCBHs (J_{crit}), if $J_{\text{crit},0} = 1500$ and $f_{\text{X}}/f_{\text{LW}} = 1$. A colour version of this figure is available in the online version.

that $J_{\text{crit},0}$ does not change significantly for $T_* \gtrsim 2 \times 10^4$ K because the typical Pop II galaxies have spectra that are flatter and harder than the thermal spectrum with $T_* = 10^4$ K (Inoue 2011). The values of $J_{\text{crit},0}$ estimated from the 3D simulations tend to be larger by one order of magnitude than that derived in one-zone models because of $\sim 20\%$ spatial variation in the temperature inside the collapsing gas clouds. The temperature fluctuations produce a large difference in the H_2 -collisional dissociation rate by one order of magnitude (Shang, Bryan & Haiman 2010). In light of this effect, it is reasonable to expect the actual value of $J_{\text{crit},0}$ to be $\gtrsim 10^3$.

The value of $J_{\text{crit},0}$ has several uncertainties beyond the FUV spectrum of the irradiating galaxies. For example, we can list uncertainties from (i) the H_2 self-shielding factor, as well as (ii) reaction rate coefficients associated with H_2 and H^- formation (see also Glover 2015). These can affect the value of $J_{\text{crit},0}$ by a factor of $\sim 3 - 4$. Therefore, in what follows, we do not specify the value of $J_{\text{crit},0}$ but regard as a free parameter, and choose instead to focus on the relative enhancement $J_{\text{crit}}/J_{\text{crit},0}$.

4 DCBH FORMATION PROBABILITY AND NUMBER DENSITY

Now, we turn to the probability that a massive halo is exposed to J_{crit} by a neighbouring galaxy, and use this quantity to estimate the number density of $z \sim 10$ seed BHs formed through FUV-aided direct collapse. The methods and calculations presented here follow those developed by DFM14. We summarize the requisite calculations below, and refer the reader to that paper for further details.

Metal pollution by galactic outflows could suppress the

Table 5. Summary of how the critical FUV intensity for DCBH formation (J_{crit}) and the corresponding formation probability (P_{DCBH}) increase when accounting for X-ray ionization. We show how these quantities change for three representative values of the X-ray-uncorrected value $J_{\text{crit},0}$ (500, 1500 and 3000); for $z = 10$ and $z = 20$; with and without metal enrichment by galactic winds (DFM14 model). These calculations assume $f_{\text{X}}/f_{\text{LW}} = 1$.

| | | UV only | UV + X |
|----------|---------|---------------------------------------|--|
| | | $J_{\text{crit},0} = 5 \times 10^2$ | $\Rightarrow J_{\text{crit}} \simeq 9 \times 10^2$ |
| $z = 10$ | w/wind | 1.6×10^{-10} | 1.2×10^{-11} |
| | no wind | 1.6×10^{-9} | 1.4×10^{-10} |
| $z = 20$ | w/wind | 5.9×10^{-7} | 1.8×10^{-8} |
| | no wind | 4.9×10^{-4} | 3.4×10^{-5} |
| | | $J_{\text{crit},0} = 1.5 \times 10^3$ | $\Rightarrow J_{\text{crit}} \simeq 7 \times 10^3$ |
| $z = 10$ | w/wind | 7.2×10^{-13} | 2.0×10^{-16} |
| | no wind | 1.2×10^{-11} | 3.1×10^{-15} |
| $z = 20$ | w/wind | 6.0×10^{-10} | 7.1×10^{-14} |
| | no wind | 2.1×10^{-6} | 1.7×10^{-10} |
| | | $J_{\text{crit},0} = 3 \times 10^3$ | $\Rightarrow J_{\text{crit}} \simeq 3 \times 10^4$ |
| $z = 10$ | w/wind | 2.1×10^{-14} | 5.0×10^{-21} |
| | no wind | 3.4×10^{-13} | 1.2×10^{-19} |
| $z = 20$ | w/wind | 7.8×10^{-12} | 5.6×10^{-18} |
| | no wind | 3.4×10^{-8} | 1.6×10^{-15} |

probability of DCBH formation because the metal cooling induces efficient gas fragmentation. We here consider the case incorporating the metal-enriching wind model of DFM14, as well as the case without winds.

We briefly describe how to calculate the PDF of J_{LW} . We define potential DCBH formation sites as atomic-cooling halos with virial temperature of $T_{\text{vir}} = 10^4$ K, corresponding to a mass $M_{\text{ac}}(z) = 8.1 \times 10^7 M_{\odot} ((1+z)/11)^{-3/2}$. A nearby star-forming galaxy can act as an FUV source for keeping H_2 photodissociated (Dijkstra et al. 2008). The differential probability distribution of finding an FUV source with mass M at a distance r is simply written

$$\frac{d^2 P_1(M, r, z)}{dM dr} = 4\pi r^2 (1+z)^3 [1 + \xi(M_{\text{ac}}, M, r, z)] \frac{dn_{\text{ST}}}{dM}, \quad (17)$$

where ξ is the non-linear bias function, which represents the clustering of the two halos (i.e. the excess probability of finding another halo at a distance r ; Iliev et al. 2003) and dn_{ST}/dM is the Sheth-Tormen halo mass function (Sheth, Mo & Tormen 2001). Furthermore, we assume a log-normal distribution for the distribution of the LW luminosity of the source galaxies,

$$\frac{dP_2(L_{\text{LW}}, M, z)}{d \log L_{\text{LW}}} = \frac{1}{\sqrt{2\pi\sigma_{\text{LW}}^2}} \times \exp \left[-\frac{(\log L_{\text{LW}} - \log \langle L_{\text{LW}} \rangle)^2}{2\sigma_{\text{LW}}^2} \right], \quad (18)$$

where $\langle L_{\text{LW}} \rangle$ is the mean LW luminosity (see equation 6 and 8 in DFM14) and $\sigma_{\text{LW}} = 0.4$ is the dispersion. While our primary motivation in choosing a log-normal distribution for L_{LW} is consistency with Dijkstra et al. (2008) and DFM14, we also note that this type of distribution is commonly used to describe populations of galaxies (e.g.

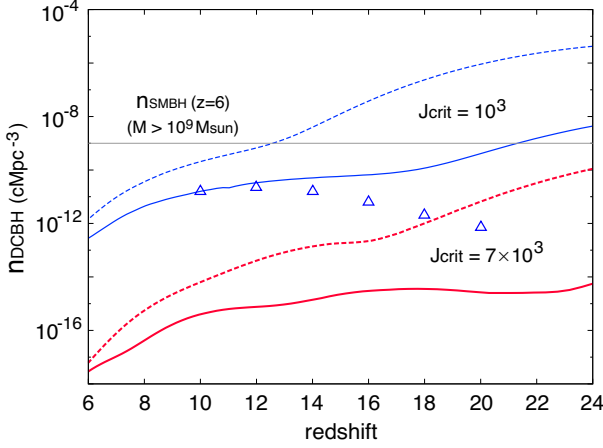


Figure 4. Redshift evolution of the number density (comoving) of forming DCBHs in atomic cooling halos. The thin (blue) and thick (red) lines show the cases that the X-ray-corrected $J_{\text{crit}} = 10^3$ and 7×10^3 , respectively. The solid and dashed lines represent the cases with and without metal-enrichment by galactic winds, respectively. The horizontal line indicates $10^{-9} \text{ cMpc}^{-3}$, which is the number density of observed SMBHs with mass $\gtrsim 10^9 M_{\odot}$ at $z \gtrsim 6$. Triangle symbols show the results for $J_{\text{crit}} = 10^3$ and with galactic winds, which are calculated using the same treatment of the nonlinear bias function as DFM14. A colour version of this figure is available in the online version.

Cooray & Milosavljević 2005; Vale & Ostriker 2008). Using the relation $L_{\text{LW}} = 16\pi^2 r^2 J_{\text{LW}}$, we obtain the PDF of a given atomic-cooling halo being exposed to a LW flux J_{LW} :

$$\frac{dP_{\text{DCBH}}(J_{\text{LW}}, z)}{d \log J_{\text{LW}}} = \int_{M_{\text{min}}}^{\infty} dM \int_{r_{\text{min}}}^{\infty} dr \frac{d^2 P_1}{dM dr} \frac{dP_2}{d \log L_{\text{LW}}}. \quad (19)$$

We set $M_{\text{min}} = M_{\text{ac}}$. For the case with metal pollution by galactic winds, we apply $r_{\text{min}} = \max(r_{\text{vir}}(M_{\text{ac}}) + r_{\text{vir}}(M), r_s(M))$, where $r_s(M)$ is the distance from the sources within which the gas is polluted by metals and DCBH formation is quenched (see equation 5 in DFM14). For the case without metal-enriching winds, we simply set $r_{\text{min}} = r_{\text{vir}}(M_{\text{ac}}) + r_{\text{vir}}(M)$. Note that DFM14 set $r_{\text{min}} = 2r_{\text{vir}}(M_{\text{ac}})$.

In Fig. 3, we show the PDF of J_{LW} for two redshifts of $z = 10$ (blue) and 20 (red). The solid and dashed lines represent the cases with and without metal pollution by galactic outflows, respectively. With (without) metal pollution⁷, $dP_{\text{DCBH}}/d \log J_{\text{LW}} \sim 8 \times 10^{-11} (9 \times 10^{-10})$ for $J_{\text{LW}} = 10^3$ at $z \simeq 10$. The PDF rapidly falls off with increasing J_{LW} . For $10^3 \lesssim J_{\text{LW},21} \lesssim 10^4$, this behavior roughly follows a power law $\propto J_{\text{LW}}^{-\beta}$ with $\beta \approx 5$.

The steep dependence of $dP_{\text{DCBH}}/d \log J_{\text{LW}}$ has a dramatic effect on the probability of DCBH formation. Using

⁷ Both values are smaller than the results shown in Fig. C1 of DFM14. We have determined that this difference is due to our choice of $r_{\text{min}} = r_{\text{vir}}(M_{\text{ac}}) + r_{\text{vir}}(M)$, which is greater than the choice $r_{\text{min}} = 2r_{\text{vir}}(M_{\text{ac}})$ adopted by DFM14. Larger r_{min} results in lower probabilities of being exposed to a given J_{LW} , since the requisite luminosity $L_{\text{LW}} \propto r^2 J_{\text{LW}}$ follows a log-normal PDF. Note that this also means that $dP_{\text{DCBH}}/d \log J_{\text{LW}}$ decreases with redshift since $r_{\text{vir}}(M_{\text{ac}}) \propto (1+z)^{-3/2}$ and $r_{\text{vir}}(M) \propto M^{1/3}(1+z)^{-1}$.

the approximation above that $dP_{\text{DCBH}}/d \log J_{\text{LW}} \propto J_{\text{LW}}^{-\beta}$ with $\beta \approx 5$, and combining this with equation (16), we can write how the X-ray-corrected PDF depends on $J_{\text{crit},0}$:

$$\frac{dP_{\text{DCBH}}(z=10)}{d \log J_{\text{LW}}} \approx \left\{ \begin{array}{l} 2 \times 10^{-15} \\ 3 \times 10^{-14} \end{array} \right\} \times \left(\frac{J_{\text{crit},0}}{1500} \right)^{-12} \left(\frac{f_{\text{X}}}{f_{\text{LW}}} \right)^{-6.7}, \quad (20)$$

where the two values inside the curly brackets correspond to cases with (top) and without (bottom) metal-enrichment. In Table 5, we summarize the values of the integrated probability $P_{\text{DCBH}}(\geq J_{\text{crit}}, z)$ for $z = 10$ and $z = 20$. As we showed in §3.2, X-ray ionizations can increase J_{crit} if the X-ray-uncorrected value is $J_{\text{crit},0} \gtrsim 500 (f_{\text{X}}/f_{\text{LW}})^{-1}$. This decreases P_{DCBH} by several orders of magnitude.

Above, we showed that soft X-rays can increase the critical FUV intensity to $J_{\text{crit}} \sim 7 \times 10^3$ if $J_{\text{crit},0}$ (the value without accounting for X-ray ionizations) is 1.5×10^3 . This results in a DCBH formation probability (per halo): $P_{\text{DCBH}} \sim 2.0 \times 10^{-16} (3.1 \times 10^{-15})$ at $z \sim 10$ with (without) metal enrichment by galactic winds. (Note that we have not accounted for enrichment via *in situ* star formation, which would further reduce P_{DCBH} .) These values are 3–4 orders of magnitude lower than the result calculated without considering soft X-rays: $P_{\text{DCBH}} \sim 7.2 \times 10^{-13} (1.2 \times 10^{-11})$. This case corresponds to an X-ray intensity $J_{\text{X},21} \simeq 0.07$ that is larger by a few orders of magnitude than that of the observed X-ray background. This is only natural, as to be exposed to FUV intensities above J_{crit} , the putative DCBH formation site must be very close to a star-forming galaxy, and therefore also exposed to strong soft X-ray intensities.

Finally, the number density (comoving) of forming DCBHs in an atomic cooling halo with mass M_{ac} is given by

$$n_{\text{DCBH}}(z) = \int_{M_{\text{ac}}}^{\infty} dM \frac{dn_{\text{ST}}}{dM} P_{\text{DCBH}}(\geq J_{\text{crit}}, z), \\ \approx n_{\text{ST}}(M \geq M_{\text{ac}}, z) P_{\text{DCBH}}(\geq J_{\text{crit}}, z). \quad (21)$$

Here, we have followed the approximations taken by DFM14, except that we have taken the factor P_{gen} (the probability that a given halo has *not* been metal-enriched by *in situ* star formation) to be unity for simplicity. Note that since $P_{\text{gen}} \leq 1$, the estimate given by equation (21) is conservative.

In Fig. 4, we show n_{DCBH} as a function of z for $J_{\text{crit}} = 10^3$ (thick red) and 7×10^3 (thin blue). The solid and dashed lines represent the cases with and without metal-enrichment by galactic winds, respectively. At $z \simeq 10$, the number density of DCBHs is smaller than that of $\gtrsim 10^9 M_{\odot}$ SMBHs observed at $z \gtrsim 6$ ($\sim 10^{-9} \text{ cMpc}^{-3}$, Willott et al. 2010; shown as a horizontal line in the figure), for all cases considered here. For $J_{\text{crit}} = 7 \times 10^3$, which corresponds to $J_{\text{crit},0} \simeq 1.5 \times 10^3$ (no X-ray ionization) for $f_{\text{X}}/f_{\text{LW}} = 1$, even the case without metal enrichment cannot exceed $10^{-9} \text{ cMpc}^{-3}$ for all redshift. We note that n_{DCBH} for the case of $J_{\text{crit}} = 10^3$ and no metal pollution can be larger than the observed value at $z \gtrsim 12$ although this is the most optimistic case (i.e. no winds and $P_{\text{gen}} = 1$).

Note that we find n_{DCBH} that increases toward higher redshifts, whereas it decreases in similar calculations by DFM14 (their Fig. 4). This is due to the fact that DFM14 computed $\xi(z=10)$, the two-point correlation function at $z = 10$, and assumed that it can be approximated at any other redshift as $\xi \approx \xi(z=10)[D_+(z)/D_+(z=10)]^2$, where

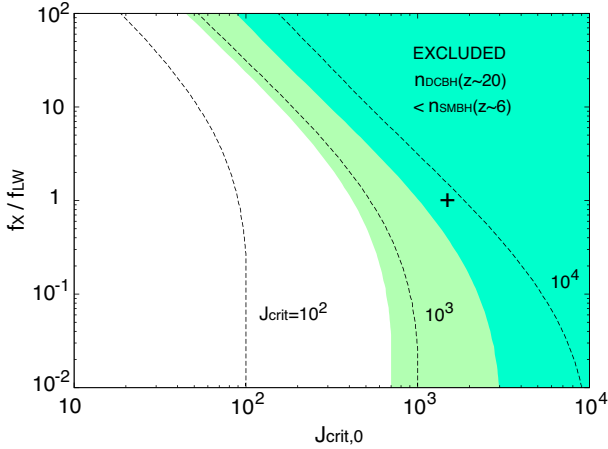


Figure 5. Contour plots of J_{crit} (including X-ray ionization) in the two-dimensional parameter space ($J_{\text{crit},0}$, f_X/f_{LW}). The shaded regions show the regions in this parameter space where the number density of DCBHs falls below the value of $\sim 10^9 M_\odot$ SMBHs observed at $z \sim 6$. The lightly (darkly) shaded region shows this space for n_{DCBH} evaluated at $z = 10$ (20), corresponding to $J_{\text{crit}} \gtrsim 700$ (3×10^3). Cross symbol indicates our fiducial model ($J_{\text{crit},0} = 1.5 \times 10^3$ and $f_X/f_{\text{LW}} = 1$). A colour version of this figure is available in the online version.

$D_+(z)$ is the growth factor. This assumption that $\xi \propto D_+^2$ is valid for the linear growth factor; however, for the non-linear growth factor formulae of Iliev et al. (2003) at small separations, ξ does not follow this relation and instead increases with z . This leads to the qualitative difference in our findings. For reference, in Fig. 4 we have overlaid with triangle symbols the n_{DCBH} estimates calculated with the same bias treatment as DFM14. Again: our calculations for n_{DCBH} increases with z , because we explicitly calculate the nonlinear bias at each redshift using the equations of Iliev et al. (2003); in contrast, DFM14 assumed $\xi(z) \propto D_+^2(z)$, which results in n_{DCBH} decreasing toward higher redshifts.

Note that for combinations of high J_{crit} and lower redshifts (e.g. $J_{\text{crit}} \gtrsim 10^3$ and $z \lesssim 15$), the characteristic halo mass where P_{DCBH} is highest can increase to $M \gg M_{\text{ac}}$. This is because r_{min} increases toward low z as described above. Since the required LW luminosity for a neighbouring halo to enable direct collapse is $L_{\text{crit}} > 16\pi^2 r_{\text{min}}^2 J_{\text{crit}}$, for cases of large J_{crit} and large r_{min} (low z) only massive neighbouring halos are able to provide such a flux. In such cases, the probability is limited not by the number of atomic-cooling halos, but by the number of massive FUV sources, and equation (21) should be evaluated using the abundances of the latter.

In Fig. 5, we show contour plots of J_{crit} (including X-ray ionization), calculated from equations (14) and the value of $J_{\text{crit}}/J_{\text{crit},0}$ for $h\nu_{\text{min}} = 1$ keV and $T_* = 3 \times 10^4$ K shown in Fig. 1, in the two-dimensional parameter space ($J_{\text{crit},0}$, f_X/f_{LW}). The shaded regions show the regions in this parameter space where the number density of DCBHs (n_{DCBH} , calculated using equation 21) falls below the value of $\sim 10^9 M_\odot$ SMBHs observed at $z \sim 6$. The lightly shaded region shows this space for n_{DCBH} evaluated at $z = 10$, corresponding to $J_{\text{crit}} \gtrsim 700$; the darkly shaded region shows where $n_{\text{DCBH}}(z = 20) < 1 \text{ cGpc}^{-3}$, corresponding to $J_{\text{crit}} \gtrsim 3 \times 10^3$. Note that these values are conservative, because they ignore metal enrichment by *in situ* star forma-

tion, as well as the decrease in the comoving number density that results from hierarchical merging of DCBH-forming halos. We therefore argue that the enhancement of J_{crit} by soft X-ray irradiation rules out this region in the physical parameter space. Most of the theoretical expectations discussed above (regarding f_X , f_{LW} and $J_{\text{crit},0}$; §3.2) point to J_{crit} being $> 10^3$.

Furthermore, we note that the requirement that the DCBH number density at $z \sim 10$ should be greater than $\sim 1 \text{ Gpc}^{-3}$ is itself also very conservative (in addition to the assumptions made regarding P_{gen}). This is because this value reflects only the abundance of $\sim 10^9 M_\odot$ SMBHs at $z \sim 6$. If one stipulates that the FUV DCBH scenario must also account for the observed $\sim 10^8 M_\odot$ SMBHs in the same redshift range, then the number density of DCBH must be at least $\sim 100 \text{ Gpc}^{-3}$ (Willott et al. 2010). All of these factors strongly put into question the viability of the FUV-aided DCBH scenario in explaining the $z \sim 6$ quasar observations.

5 DISCUSSION AND CONCLUSIONS

In this paper, we investigated the effect of X-ray irradiation on direct collapse black hole (DCBH) formation via far-ultraviolet (FUV) irradiation. X-ray ionization promotes the H_2 formation because H_2 molecules are produced by the electron-catalyzed reactions (equation 2). Thus, X-ray irradiation increases the critical FUV flux J_{crit} required to suppress the H_2 formation and cooling. Specifically, we focused on the effects of soft (~ 1 keV) X-rays emitted by the same galaxies close-proximity star-forming galaxies that provide the large FUV intensities necessary for direct collapse. Our main findings are as follows:

(i) **Galaxies supplying large J_{LW} should also provide a large soft X-ray intensity J_X .** If $z > 10$ star-forming galaxies have the same X-ray-to-FUV emission ratio as observed in their lower-redshift counterparts, then an FUV intensity $J_{\text{LW},21}$ of several 10^3 or higher would be accompanied by a soft X-ray intensity $J_{X,21} > 0.01$ (equation 14).

(ii) **Such X-ray intensities increase J_{crit} by promoting H_2 formation.** Soft X-ray intensities ($J_{X,21} > 0.01$) are sufficient to increase J_{crit} by a factor of a few or more, even under the conservative assumption that the X-ray-to-FUV ratio does not evolve with redshift. This finding agrees with that of Latif et al. (2015), who considered a background of hard 2 – 10 keV X-rays. Whereas $J_{X,21} > 0.01$ is unlikely for a cosmic X-ray background, it is plausibly the norm for putative DCBH sites.

(iii) **This change in J_{crit} results in a drop of several orders of magnitude in the DCBH abundance, compared to calculations that neglect the X-ray intensity.** The point that J_{crit} may be too high (and DCBH sites too rare) to account for the high-redshift quasar observations was previously raised by DFM14. Our results imply that accounting for the soft X-rays produced locally—by the very same galaxies that supply the photodissociating FUV photons necessary for direct collapse—places an additional stress on the viability of the DCBH model to explain SMBH formation in general.

We stress two points. The first point is that this X-ray enhancement of J_{crit} is a general effect. Our calculations utilized several simplifying assumptions. For one, we relied on one-zone estimates that do not include three-dimensional effects (e.g. turbulence, anisotropy, and inhomogeneity) and detailed hydrodynamics. For another, our semi-analytic estimates of galaxy/SMBH number densities at high redshifts (following DFM14) suffer from uncertainties in the properties of the earliest stars and galaxies. While improvements on these areas will surely lead to a more realistic quantitative estimate of J_{crit} and n_{DCBH} , we expect our main findings enumerated above to be qualitatively robust. This is precise the reason that in many parts of this paper we treat the X-ray-uncorrected critical FUV intensity $J_{\text{crit},0}$ (which could change with improved physical modeling, as well as vary from one potential DCBH site to another) as a loose parameter, and instead focus on the X-ray enhancement factor $J_{\text{crit}}/J_{\text{crit},0}$.

The second point of note is that this effect is highly likely to be astrophysically relevant. We have adopted conservative parameter values in estimating the X-ray intensity due to the FUV source galaxies. As stated above: the X-ray intensity $J_{X,21} \sim 10^{-2}$ required to affect J_{crit} (see Figs. 1 and 2), while much higher than the cosmic X-ray background, should be fairly typical for putative DCBH formation sites with $J_{\text{LW},21} > 10^3$. If direct collapse requires $J_{\text{LW},21} \sim 10^4$ (as suggested by the most recent simulations), $J_{X,21}$ would be $\sim 10^{-1}$. The actual X-ray intensity could be still higher if star-forming galaxies at $z > 10$ produced more $\sim 1 - 2$ keV X-rays relative to FUV photons (i.e. $f_X/f_{\text{LW}} > 1$)—due to higher HMXB activity.

5.1 Constraints from 21 cm observations

We have shown that X-ray ionizations may play a powerful role in suppressing FUV-aided DCBH formation. As shown in §4 (Figs. 4 and 5), the predicted number density of DCBHs at $z \simeq 10 - 20$ for $f_X \gtrsim 1$ can be much less than that of the observed high- z QSOs with $M \sim 10^9 M_\odot$, ~ 1 comoving Gpc^{-3} (or ~ 100 comoving Gpc^{-3} for $M \gtrsim 10^8 M_\odot$ SMBHs). For $f_X \gtrsim 0.1$, if $J_{\text{crit},0} \gtrsim 2 \times 10^3$, FUV-DCBH formation is ruled out as it cannot make enough seed BHs at $10 < z < 20$ to account for the observed $z \sim 6$ quasar population. However, the possibility that f_X is much smaller than 0.1 is not excluded by current observational data.

The 21-cm line transition of neutral hydrogen is one of the most promising observations to probe the thermal history of the intergalactic medium before the cosmic reionization. Future observations of 21-cm signals from the high- z Universe could give a lower limit on f_X and thus help to further test the viability of the FUV-DCBH scenario. The power spectrum of the brightness temperature of the 21-cm line at the scale of $\simeq 0.1 \text{ Mpc}^{-1}$ has three peaks as a function of redshift (e.g., Pritchard & Furlanetto 2007; Mesinger, Ferrara & Spiegel 2013; Christian & Loeb 2013). The location and amplitude of the second peak is sensitive to the value of f_X . As the X-ray intensity is weaker than that from star-forming galaxies at the low- z universe ($f_X \ll 0.1$), the peak position shifts toward lower-redshift and its amplitude becomes larger. In this case, the 21-cm signal can be observed by 1st-generation interferometers; e.g. the Low Frequency Array (LOFAR, van Haarlem et al. 2013) and

Murchison Wide Field Array (MWA, Tingay et al. 2013). On the other hand, for stronger X-ray intensities ($f_X \gg 0.1$), the spin temperature approaches the CMB temperature due to X-ray heating at higher redshift. Then, the peak of 21-cm signal moves to higher redshift and becomes smaller.

Second generation interferometers such as the Square Kilometre Array (SKA, Mellema et al. 2013) will be required to observe the signal for larger f_X . However, near-future observations will be able to impose a lower limit of X-rays in the early Universe around $f_X \sim 0.1$ (e.g., Christian & Loeb 2013; Mesinger, Ewall-Wice & Hewitt 2014). The same observations should also be able to constrain the efficacy of SMBH growth through rapid growth of Pop III remnants (Tanaka, O’Leary & Perna, in prep.).

5.2 Co-production of X-ray and FUV radiation

In this paper, we assume that star-forming galaxies emit X-rays as well as FUV radiation. This assumption seems reasonable when star formation occurs continuously during the cosmic time at the high- z Universe (~ 300 Myr for $z \sim 15$), because the lifetime of massive stars is shorter than ~ 10 Myr. The lifetime t_{life} of massive stars with mass of $15/25/40/200 M_\odot$ is $10/6.5/3.9/2.2$ Myr (Schaerer 2002). Observations of star-forming galaxies at lower redshift also support this assumption (e.g., Mineo, Gilfanov & Sunyaev 2012, and references therein). The co-production of X-rays with FUV photons is also seemingly unavoidable when a galaxy or an atomic-cooling halo undergoes an intense and short burst of star formation. Because some fraction of the newly formed stars will die and form HMXBs, there may be a very narrow window (at most $t_{\text{life}} \sim$ a few Myr) inside which a DCBH forming halo is irradiated by FUV radiation but not X-rays.

Let us also consider the gas properties inside a DCBH-forming halo. The gas density at the central core, before radiative cooling operates, is $\lesssim 10 \text{ cm}^{-3} ((1+z)/11)^3$ (Visbal, Haiman & Bryan 2014a). After the virial temperature reaches $\gtrsim 8000$ K, H atomic cooling causes the gas to undergo gravitational collapse. Since the density increases on the free-fall timescale, it will take $t_{\text{coll}} \gtrsim 20$ Myr $((1+z)/11)^{-3/2}$ for the gas density to exceed $\sim 10^3 \text{ cm}^{-3}$ —the value where H_2 molecules can be collisionally dissociated instead of by FUV irradiation. Then it follows that X-ray irradiation must accompany any strong FUV intensity as long as $t_{\text{life}} < t_{\text{coll}}$.

Recently, Visbal, Haiman & Bryan (2014b) proposed a new DCBH formation scenario, which considers synchronised pairs of pristine atomic cooling halos having a small separation $\lesssim 0.5$ kpc. If one of the halos reaches the atomic cooling threshold (i.e., $T_{\text{vir}} \gtrsim 8000$ K) just after star formation occurs in another halo, the first halo can be irradiated with the critical FUV intensity due to a small separation (SFR $\sim 0.05 M_\odot \text{ yr}^{-1}$ is required to realize $J_{\text{crit},0} \sim 2 \times 10^3$). To be viable, this scenario must keep the gas free of ionizing X-rays and metal-enriching winds for a collapse timescale ~ 20 Myr $((1+z)/11)^{-3/2}$. As argued above, the FUV-producing massive stars can become X-ray sources on a significantly shorter timescale t_{life} . Thus, we argue that X-ray irradiation can also suppress this “synchronised pair” scenario. (Also note that the timescale on which winds can reach and pollute the gas is

also comparable to t_{coll} ; DFM14.) However, these arguments (lifetime of massive stars, photo-evaporation, and metal pollution) depend on a number of uncertain parameters (e.g. initial mass function, star formation efficiency, clumping factor of the intergalactic medium, and wind velocity). We also note that the X-ray luminosity estimated from equation (11) is $\sim 3.4 \times 10^{38}$ (SFR/0.05 $M_{\odot} \text{ yr}^{-1}$) erg s^{-1} , which is a few times the Eddington luminosity of stellar mass BH. This fact implies that only a handful of luminous X-ray binaries are required to achieve $J_{\text{crit},0}$ in this particular case, and that X-ray luminosities in such low-mass halos may have a dispersion larger than the ~ 0.4 dex value found in more massive galaxies. A finer knowledge of these details will be required to better understand the impact of various photon sources inside such close, synchronised halo pairs.

5.3 Other effects to enhance J_{crit} and suppress the DCBH formation

We here discuss the suppression of DCBH formation by other ionization effects. In the early universe, the promising ionizing radiations other than X-rays are cosmic rays (CRs) and EUV photons (≥ 13.6 eV) from star-forming galaxies. These sources of radiation increase the ionization fraction of the gas in the atomic cooling halos where SMSs would be born. Thus, they should also increase the requisite FUV intensity for DCBH formation, in much the same way as the effect of X-ray ionizations discussed in this work.

The enhancement of J_{crit} by CR ionization operates when the ionization rate is larger than $\sim 10^{-18} \text{ s}^{-1}$ at H column densities of $\sim 10^{22} \text{ cm}^{-2}$, which corresponds to $n \sim 10^3 \text{ cm}^{-3}$ and $T \sim 8000 \text{ K}$ (Inayoshi & Omukai 2011). Assuming the CR energy distribution comprises a power-law spectrum of $dn_{\text{CR}}/dE \propto E^{-2}$ with $10^6 \leq E \leq 10^{15} \text{ eV}$, the ionization rate required to increase J_{crit} can be estimated as $\zeta_{\text{CR}} \gtrsim 10^{-17} \text{ s}^{-1}$, which is smaller than that observed in Milky Way, $10^{-17} \lesssim \zeta_{\text{CR}} \lesssim 10^{-15} \text{ s}^{-1}$ (Hayakawa, Nishimura & Takayanagi 1961; Spitzer & Tomasko 1968; Webber 1998; McCall et al. 2003; Indriolo et al. 2007). According to theoretical estimate (e.g. Stacy & Bromm 2007; Inayoshi & Omukai 2011; Nakauchi, Inayoshi & Omukai 2014), the CR ionization rate is

$$\zeta_{\text{CR}} \sim 2 \times 10^{-20} \text{ s}^{-1} \left(\frac{d}{10 \text{ kpc}} \right)^{-2} \left(\frac{\text{SFR}}{M_{\odot} \text{ yr}^{-1}} \right), \quad (22)$$

where we assume that 10 per cent of the supernovae explosion energy ($E_{\text{SN}} = 10^{51} \text{ erg}$) converts to the CR acceleration and the Salpeter initial mass function as we assumed for the FUV intensity. Combining equation (22) and $J_{\text{LW},21} = f_{\text{LW}} \bar{J}_{\text{LW},21}$, then we can find

$$\zeta_{\text{CR}} \sim 2 \times 10^{-19} \text{ s}^{-1} f_{\text{LW}}^{-1} \left(\frac{J_{\text{LW},21}}{10^3} \right), \quad (23)$$

which is smaller than the ionization rate above which J_{crit} increases. However, the CR intensity in the early universe has uncertainties associated with magnetic fields, e.g., the confinement of CRs in star-forming galaxies and CR propagation in the intergalactic medium (e.g. Strong, Moskalenko & Ptuskin 2007, and references therein). Thus, more sophisticated models are required to

better evaluate the impact of CR ionizations on DCBH formation.

EUV photons with ≥ 13.6 eV can easily be absorbed by the intergalactic medium because their optical depth in neutral hydrogen is as large as

$$\tau_{\text{H}}(\nu) \sim 10^4 \left(\frac{n}{1.0 \text{ cm}^{-3}} \right)^{1/2} \left(\frac{h\nu}{13.6 \text{ eV}} \right)^{-3}. \quad (24)$$

Thus, EUV photons cannot penetrate into the dense and hot region ($n \sim 10^3 \text{ cm}^{-3}$ and $T \simeq 8000 \text{ K}$) in atomic cooling halos. As a result, the critical FUV intensity does not change because of self-shielding to EUV photons. However, EUV photons would suppress DCBH formation during and after cosmic reionization, only when the gas around atomic-cooling halos becomes ionized completely (Yue et al. 2014; Johnson et al. 2014).

5.4 Alternative models forming DCBHs

We discuss alternative scenarios of forming DCBHs which do not require strong FUV radiation. The relevant H_2 dissociating process instead of FUV photodissociation is collisional dissociation ($\text{H}_2 + \text{H} \rightarrow 3\text{H}$). In atomic cooling halos ($T_{\text{vir}} \gtrsim 10^4 \text{ K}$), this process works efficiently in case that the gas density and temperature are $n \gtrsim 10^4 \text{ cm}^{-3}$ and $T \gtrsim 6000 \text{ K}$, respectively. Once the primordial gas enters such a dense and hot region (so-called ‘‘zone of no return’’), the H_2 formation/cooling is quenched by the collisional dissociation even *without FUV radiation* enough for the gas to collapse keeping a high temperature ($\sim 8000 \text{ K}$) by H-atomic cooling (Inayoshi & Omukai 2012).

One promising process for forming such a dense and hot gas is strong shock by collisions of cold accretion flows due to assembly of the first galaxies. Since the radiative cooling of the gas is efficient in the first galaxies, the gas can penetrate deep to the centre ($\sim 0.1 R_{\text{vir}}$) as dense filamentary inflows. If the cold flows jump into the zone of no return by shock heating, a supermassive star can form from the parent cloud in the post-shock region. However, supersonic filamentary flows are unlikely to be dense before experiencing shocks for weak-cooling case ($T_{\text{vir}} \lesssim 8000 \text{ K}$; Fernandez et al. 2014) and no-cooling case (Visbal, Haiman & Bryan 2014a). These two examples suggest that massive halos ($T_{\text{vir}} \gtrsim 10^4 \text{ K}$) could be necessary for the gas to arrive in the zone of no return. To better understand the actual probability of a dense shocked gas cloud forming in this way, a large, statistical sample of numerical simulations of atomic-cooling halos is required.

A galaxy merger is another mechanism that can induce strong inflows and form an environment similar to the one made by the cold accretion shocks. Mayer et al. (2010) performed a numerical simulation of the merger between massive ($\sim 10^{12} M_{\odot}$) and metal-enriched ($\sim Z_{\odot}$) protogalaxies at $z \sim 6$, assuming a simple polytropic equation of state (i.e., $p \propto \rho^{\gamma}$). After the merging, the gravitationally unstable disc is formed, where the non-axisymmetric structures (spiral arms and bars) transport the gas angular momentum efficiently. In that case, strong inflows rapidly accumulate a mount of gas with $10^8 M_{\odot}$ within the central pc scale. The average density of the nuclear region reaches $\sim 10^9 \text{ cm}^{-3}$, at which point H_2 molecules can remain collisionally dissociated. However, Ferrara, Haardt & Salvaterra

(2013) have noted that the gas actually fragments into clumps with $\lesssim M_{\odot}$ if one considers more realistic radiative cooling prescriptions, instead of a simple equation of state. Volonteri & Begelman (2010) discussed the possibility that gas can accumulate in the galaxy center due to rapid angular momentum transfer via bar instabilities, as long as the mass inflow rate is higher than the star formation rate. Further research is required to determine whether the galaxy merger could produce massive clouds forming DCBHs, when fully accounting for the cooling and chemical reactions of primordial gas.

A third avenue for forming DCBHs without FUV radiation was recently proposed by Tanaka & Li (2014). The relative bulk streaming motion between baryons and dark matter left over from cosmic recombination (Tselikhovich & Hirata 2010) has been shown to delay gas infall and Pop III star formation in $z \gtrsim 20$ halos with $T_{\text{vir}} \sim 1000 - 2000$ K (Stacy, Bromm & Loeb 2011; Greif et al. 2011; Fialkov et al. 2012; Naoz, Yoshida & Gnedin 2013). Tanaka & Li noted that in rare combinations of particularly massive halos and exceptionally large streaming velocities, the delay in gas infall may persist until the halo reaches $T_{\text{vir}} \sim 8000$ K. Gas falling into such halos would naturally shock to 8000 K before ever forming stars. The gas will undergo direct collapse if it can reach sufficiently large densities to keep H_2 collisionally dissociated (however, note the caveats and uncertainties discussed above). Tanaka & Li (2014) predicted that this mechanism a characteristic redshift $z \sim 30$, where the product of the atomic-cooling halo number density and the probability of having a sufficiently large streaming velocity (i.e. significant delay in gas infall) is maximized.

5.5 The Effect of Metallicity

We briefly consider the possibility that the effect discussed in this paper could be alleviated by the absorption of X-rays by heavy elements (present in the interstellar or circumgalactic medium of the FUV/X-ray source galaxy). Indeed, the total cross section of metals in the interstellar medium is larger than those of H and He by 1 – 2 orders of magnitude at 1 – 10 keV, at solar abundances (e.g. Morrison & McCammon 1983). However, the metallicities in the environments of interest here are likely to be much lower than solar. For $Z \lesssim 10^{-3} Z_{\odot}$, the contribution of metals to the optical depth is less than 10 per cent, and absorption by metals is unlikely to shield the putative DCBH formation sites from X-rays.

ACKNOWLEDGEMENTS

We thank Mark Dijkstra, Zoltán Haiman, Eli Visbal, Kazuyuki Omukai and Kazuyuki Sugimura for fruitful discussions, as well as Jarrett L. Johnson, Muhammad Latif, Dominik Schleicher, and Marta Volonteri for comments on the manuscript. We also thank Akio Inoue for providing the data of the spectral model of Pop II galaxies. This work is partially supported by Grants-in-Aid from the Ministry of Education, Culture, and Science of Japan (to KI).

REFERENCES

- Agarwal B., Khochfar S., Johnson J. L., Neistein E., Dalla Vecchia C., Livio M., 2012, *MNRAS*, 425, 2854
- Alvarez M. A., Wise J. H., Abel T., 2009, *ApJL*, 701, L133
- Bañados E. et al., 2014, *AJ*, 148, 14
- Basu-Zych A. R. et al., 2013, *ApJ*, 762, 45
- Becerra F., Greif T. H., Springel V., Hernquist L. E., 2015, *MNRAS*, 446, 2380
- Begelman M. C., Volonteri M., Rees M. J., 2006, *MNRAS*, 370, 289
- Bromm V., Loeb A., 2003, *ApJ*, 596, 34
- Chandrasekhar S., 1964, *ApJ*, 140, 417
- Christian P., Loeb A., 2013, *J. Cosmol. Astropart. Phys.*, 9, 14
- Cooray A., Milosavljević M., 2005, *ApJL*, 627, L89
- Dijkstra M., Ferrara A., Mesinger A., 2014, *MNRAS*, 442, 2036 (DFM14)
- Dijkstra M., Gilfanov M., Loeb A., Sunyaev R., 2012, *MNRAS*, 421, 213
- Dijkstra M., Haiman Z., Mesinger A., Wyithe J. S. B., 2008, *MNRAS*, 391, 1961
- Fan X., 2006, *New Astron. Rev.*, 50, 665
- Fan X. et al., 2001, *AJ*, 122, 2833
- Fernandez R., Bryan G. L., Haiman Z., Li M., 2014, *MNRAS*, 439, 3798
- Ferrara A., Haardt F., Salvaterra R., 2013, *MNRAS*, 434, 2600
- Ferrarese L., Merritt D., 2000, *ApJL*, 539, L9
- Fialkov A., Barkana R., Tselikhovich D., Hirata C. M., 2012, *MNRAS*, 424, 1335
- Fragos T. et al., 2013a, *ApJ*, 764, 41
- Fragos T., Lehmer B. D., Naoz S., Zezas A., Basu-Zych A., 2013b, *ApJL*, 776, L31
- Furlanetto S. R., 2006, *MNRAS*, 371, 867
- Furlanetto S. R., Oh S. P., Briggs F. H., 2006, *Physics Reports*, 433, 181
- Gierlinski M., Zdziarski A. A., Done C., Johnson W. N., Ebisawa K., Ueda Y., Haardt F., Philips B. F., 1997, *MNRAS*, 288, 958
- Gierliński M., Zdziarski A. A., Poutanen J., Coppi P. S., Ebisawa K., Johnson W. N., 1999, *MNRAS*, 309, 496
- Glover S., 2015, *ArXiv e-prints*
- Glover S. C. O., Brand P. W. J. L., 2003, *MNRAS*, 340, 210
- Greif T. H., White S. D. M., Klessen R. S., Springel V., 2011, *ApJ*, 736, 147
- Grimm H.-J., Gilfanov M., Sunyaev R., 2003, *MNRAS*, 339, 793
- Haiman Z., Loeb A., 2001, *ApJ*, 552, 459
- Hayakawa S., Nishimura S., Takayanagi T., 1961, *PASJ*, 13, 184
- Hirano S., Hosokawa T., Yoshida N., Umeda H., Omukai K., Chiaki G., Yorke H. W., 2014, *ApJ*, 781, 60
- Hopkins P. F., Hernquist L., Cox T. J., Robertson B., Krause E., 2007, *ApJ*, 669, 67
- Hosokawa T., Omukai K., Yorke H. W., 2012, *ApJ*, 756, 93
- Hosokawa T., Omukai K., Yoshida N., Yorke H. W., 2011, *Science*, 334, 1250
- Hosokawa T., Yorke H. W., Inayoshi K., Omukai K., Yoshida N., 2013, *ApJ*, 778, 178
- Hummel J. A., Stacy A., Jeon M., Oliveri A., Bromm V., 2014, *ArXiv e-prints*
- Iliev I. T., Scannapieco E., Martel H., Shapiro P. R., 2003, *MNRAS*, 341, 81
- Inayoshi K., Hosokawa T., Omukai K., 2013, *MNRAS*, 431, 3036
- Inayoshi K., Omukai K., 2011, *MNRAS*, 416, 2748
- , 2012, *MNRAS*, 422, 2539
- Inayoshi K., Omukai K., Tasker E., 2014, *MNRAS*, 445, L109
- Indriolo N., Geballe T. R., Oka T., McCall B. J., 2007, *ApJ*, 671, 1736
- Inoue A. K., 2011, *MNRAS*, 415, 2920
- Johnson J. L., Whalen D. J., Agarwal B., Paardekooper J.-P., Khochfar S., 2014, *MNRAS*, 445, 686

- Kormendy J., Ho L. C., 2013, *ARA&A*, 51, 511
- Koushiappas S. M., Bullock J. S., Dekel A., 2004, *MNRAS*, 354, 292
- Larson R. B., 1969, *MNRAS*, 145, 271
- Latif M. A., Bovino S., Grassi T., Schleicher D. R. G., Spaans M., 2015, *MNRAS*, 446, 3163
- Latif M. A., Bovino S., Van Borm C., Grassi T., Schleicher D. R. G., Spaans M., 2014, *MNRAS*, 443, 1979
- Latif M. A., Schleicher D. R. G., Schmidt W., Niemeyer J., 2013, *MNRAS*, 433, 1607
- Lehmer B. D., Alexander D. M., Bauer F. E., Brandt W. N., Goulding A. D., Jenkins L. P., Ptak A., Roberts T. P., 2010, *ApJ*, 724, 559
- Lehmer B. D. et al., 2008, *ApJ*, 681, 1163
- Li Y. et al., 2007, *ApJ*, 665, 187
- Lodato G., Natarajan P., 2006, *MNRAS*, 371, 1813
- Loeb A., Rasio F. A., 1994, *ApJ*, 432, 52
- Madau P., Rees M. J., 2001, *ApJL*, 551, L27
- Magorrian J. et al., 1998, *AJ*, 115, 2285
- Marconi A., Hunt L. K., 2003, *ApJL*, 589, L21
- Mayer L., Kazantzidis S., Escala A., Callegari S., 2010, *Nature*, 466, 1082
- McCall B. J. et al., 2003, *Nature*, 422, 500
- Mellema G. et al., 2013, *Experimental Astronomy*, 36, 235
- Mesinger A., Ewall-Wice A., Hewitt J., 2014, *MNRAS*, 439, 3262
- Mesinger A., Ferrara A., Spiegel D. S., 2013, *MNRAS*, 431, 621
- Milosavljević M., Couch S. M., Bromm V., 2009, *ApJL*, 696, L146
- Mineo S., Gilfanov M., Lehmer B. D., Morrison G. E., Sunyaev R., 2014, *MNRAS*, 437, 1698
- Mineo S., Gilfanov M., Sunyaev R., 2012, *MNRAS*, 419, 2095
- Mirabel I. F., Dijkstra M., Laurent P., Loeb A., Pritchard J. R., 2011, *A&A*, 528, A149
- Morrison R., McCammon D., 1983, *ApJ*, 270, 119
- Mortlock D. J. et al., 2011, *Nature*, 474, 616
- Nakauchi D., Inayoshi K., Omukai K., 2014, *MNRAS*, 442, 2667
- Naoz S., Yoshida N., Gnedin N. Y., 2013, *ApJ*, 763, 27
- Oh S. P., 2001, *ApJ*, 553, 499
- Oh S. P., Haiman Z., 2002, *ApJ*, 569, 558
- Omukai K., 2001, *ApJ*, 546, 635
- Omukai K., Schneider R., Haiman Z., 2008, *ApJ*, 686, 801
- Osterbrock D. E., 1989, *Astrophysics of gaseous nebulae and active galactic nuclei*
- Penston M. V., 1969, *MNRAS*, 144, 425
- Power C., Wynn G. A., Combet C., Wilkinson M. I., 2009, *MNRAS*, 395, 1146
- Pritchard J. R., Furlanetto S. R., 2007, *MNRAS*, 376, 1680
- Regan J. A., Haehnelt M. G., 2009a, *MNRAS*, 396, 343
- , 2009b, *MNRAS*, 393, 858
- Ricotti M., Ostriker J. P., 2004, *MNRAS*, 352, 547
- Rybicki G. B., Lightman A. P., 1979, *Radiative processes in astrophysics*
- Schaerer D., 2002, *A&A*, 382, 28
- , 2003, *A&A*, 397, 527
- Schleicher D. R. G., Palla F., Ferrara A., Galli D., Latif M., 2013, *A&A*, 558, A59
- Shang C., Bryan G. L., Haiman Z., 2010, *MNRAS*, 402, 1249
- Sheth R. K., Mo H. J., Tormen G., 2001, *MNRAS*, 323, 1
- Shibata M., Shapiro S. L., 2002, *ApJL*, 572, L39
- Shull J. M., van Steenberg M. E., 1985, *ApJ*, 298, 268
- Spitzer, Jr. L., Tomasko M. G., 1968, *ApJ*, 152, 971
- Stacy A., Bromm V., 2007, *MNRAS*, 382, 229
- , 2013, *MNRAS*, 433, 1094
- Stacy A., Bromm V., Loeb A., 2011, *ApJL*, 730, L1
- Stacy A., Greif T. H., Bromm V., 2012, *MNRAS*, 422, 290
- Strong A. W., Moskalenko I. V., Ptuskin V. S., 2007, *Annual Review of Nuclear and Particle Science*, 57, 285
- Sugimura K., Omukai K., Inoue A. K., 2014, *MNRAS*, 445, 544
- Susa H., Hasegawa K., Tominaga N., 2014, *ApJ*, 792, 32
- Swartz D. A., Ghosh K. K., Tennant A. F., Wu K., 2004, *ApJS*, 154, 519
- Tanaka T., Haiman Z., 2009, *ApJ*, 696, 1798
- Tanaka T., Perna R., Haiman Z., 2012, *MNRAS*, 425, 2974
- Tanaka T. L., 2014, *ArXiv e-prints*: 1406.3023
- Tanaka T. L., Li M., 2014, *MNRAS*, 439, 1092
- Tanaka T. L., Li M., Haiman Z., 2013, *MNRAS*, 435, 3559
- Tingay S. J. et al., 2013, *PASA*, 30, 7
- Tseliakhovich D., Hirata C., 2010, *Phys. Rev. D*, 82, 083520
- Vale A., Ostriker J. P., 2008, *MNRAS*, 383, 355
- van Haarlem M. P. et al., 2013, *A&A*, 556, A2
- Venemans B. P. et al., 2013, *ApJ*, 779, 24
- Verner D. A., Ferland G. J., Korista K. T., Yakovlev D. G., 1996, *ApJ*, 465, 487
- Visbal E., Haiman Z., Bryan G. L., 2014a, *MNRAS*, 442, L100
- , 2014b, *MNRAS*, 445, 1056
- Volonteri M., Begelman M. C., 2010, *MNRAS*, 409, 1022
- Volonteri M., Haardt F., Madau P., 2003, *ApJ*, 582, 559
- Volonteri M., Rees M. J., 2006, *ApJ*, 650, 669
- Webber W. R., 1998, *ApJ*, 506, 329
- Willott C. J. et al., 2010, *AJ*, 139, 906
- Wolcott-Green J., Haiman Z., Bryan G. L., 2011, *MNRAS*, 418, 838
- Yan M., Sadeghpour H. R., Dalgarno A., 1998, *ApJ*, 496, 1044
- Yue B., Ferrara A., Salvaterra R., Xu Y., Chen X., 2014, *MNRAS*, 440, 1263
- Zeldovich Y. B., Novikov I. D., 1971, *Relativistic astrophysics. Vol.1: Stars and relativity*

APPENDIX A: INCREASE OF THE ELECTRON FRACTION BY X-RAYS

In this Appendix, we discuss the effect of X-ray irradiation on thermal evolution of a collapsing gas cloud via the enhancement of the electron fraction x_e . This is a key underlying point of this paper.

Each panel of Fig. A1 shows the temperature (a), electron fraction (b), H_2 fraction (c), and H^- fraction (d) as a function of the number density, respectively. To see the effect of X-ray ionization, we first fix the FUV intensity to $J_{LW,21} = 10^4$ with a brightness temperature of 3×10^4 K. Each line represents the case of $J_{X,21} = 10^{-3}$ (solid), 10^{-2} (long dashed), 4.4×10^{-2} (short dashed), and 10^{-1} (dotted). We note that the case $J_{X,21} = 4.4 \times 10^{-2}$ corresponds to our fiducial case for $J_{LW,21} = 10^4$ (i.e. $f_X/f_{LW} = 1$ in equation 14). The dependence of J_{crit} on J_X can be found in Fig. 2, with the middle (green) solid line representing the case $T_* = 3 \times 10^4$ K discussed in this Appendix.

From Fig. A1 (a), we see how the X-ray intensity affects thermal evolution. For the weakest X-ray case ($J_{X,21} = 10^{-3}$; red solid curve), the temperature increases almost adiabatically with the gas density ($T \propto n^{2/3}$). After heating up to 10^4 K, the gas collapses isothermally ($\simeq 8000$ K) via atomic-hydrogen cooling. With stronger X-ray intensities, at low densities ($\lesssim 10 \text{ cm}^{-3}$) the temperature increases more rapidly due to X-ray photoheating. At higher densities ($\gtrsim 10^3 \text{ cm}^{-3}$), however, the gas cools down to $\sim 10^3$ K for $J_{X,21} = 4.4 \times 10^{-2}$ (blue short-dashed curve) and $J_{X,21} = 0.1$ (purple dotted). The sudden drop of the temperature is caused by H_2 cooling, which is promoted by X-ray ionization through the electron-catalyzed reactions (eqs. 1 and 2).

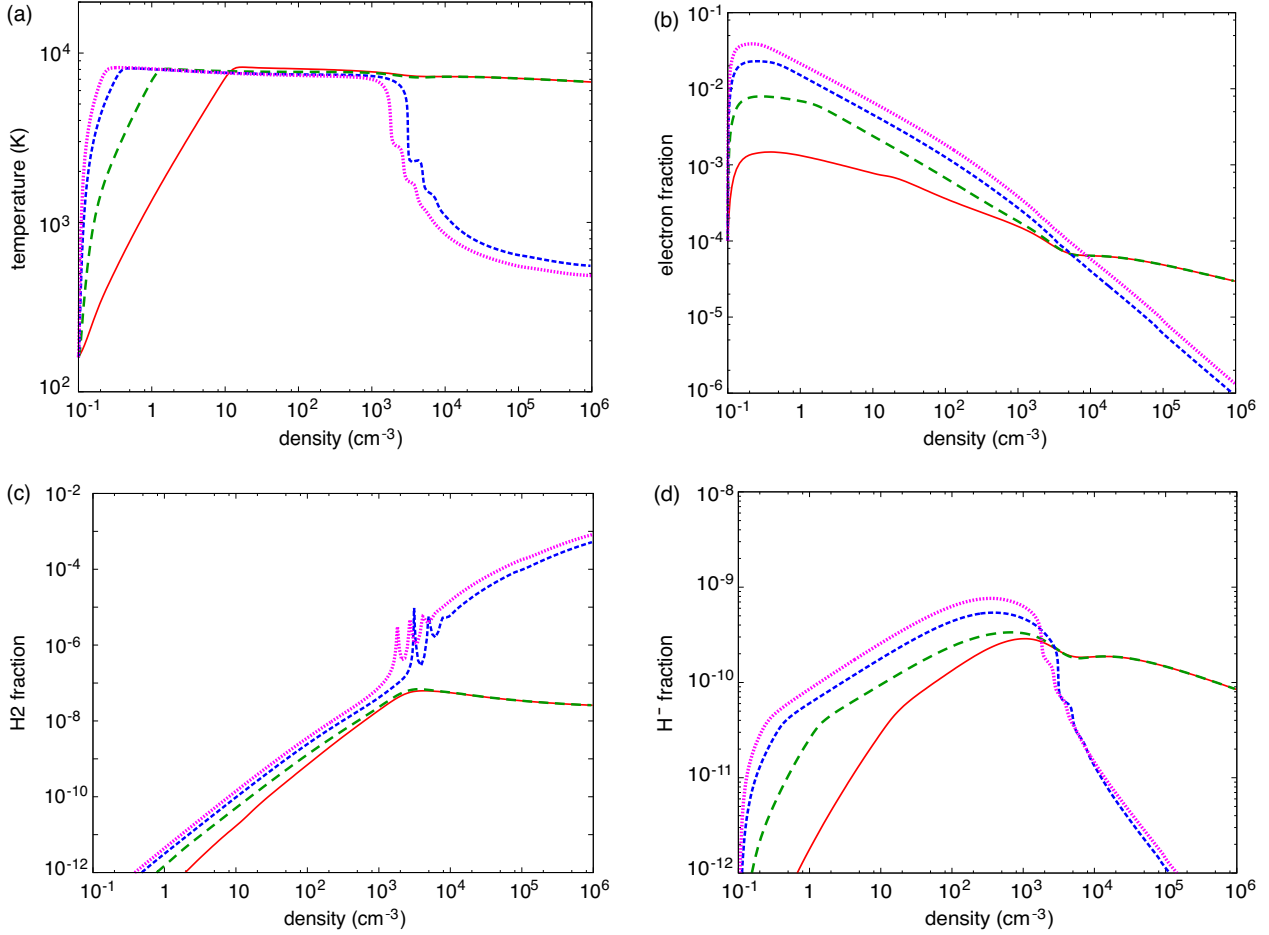


Figure A1. Evolution of the (a) temperature, (b) electron fraction, (c) H₂ fraction, and (d) H[−] fraction in a collapsing cloud irradiated by FUV radiation with $J_{\text{LW},21} = 10^4$ for $T_* = 3 \times 10^4$ K and X-rays with $J_{\text{X},21} = 10^{-3}$ (red solid), 10^{-2} (green long-dashed), 4.4×10^{-2} (blue short-dashed) and 10^{-1} (purple dotted). A colour version of this figure is available in the online version.

Fig. A1 (b) shows that the electron fraction x_e decreases as the cloud collapses, with radiative recombination balancing X-ray ionization. For the cases with weaker X-rays (red solid and green long-dashed), at large densities $n \gtrsim 10^4 \text{ cm}^{-3}$ the gas keeps a high temperature of $\simeq 8000$ K, with x_e eventually converging to a value $\simeq 4 \times 10^{-5}$. For stronger X-ray intensities (blue short-dashed and purple dotted), the electron fraction increases by X-ray ionization past $n \sim 10^3 \text{ cm}^{-3}$. This is roughly the density value at which the bifurcation of thermal evolution is determined—i.e., whether the gas remains H₂-free and nearly isothermal at ~ 8000 K, or forms H₂ and cools. Due to the enhancement of x_e , more H₂ molecules (as well as H[−] ions) form before the bifurcation point (Fig. A1 c and d).

Next, we clarify the dependence of that the critical FUV on the X-ray intensity (i.e. $J_{\text{crit}} \propto J_{\text{X},21}^b$; $b \simeq 0.5$). In Fig. A2, we show the evolution of the electron fraction again, for X-ray intensities $J_{\text{X},21} = 10^{-4}, 10^{-3}, 10^{-2}, 10^{-1}$ and 1 (from the bottom to the top). For each value of $J_{\text{X},21}$ represented in the figure, we have set the FUV intensity $J_{\text{LW},21}$ slightly higher than the critical value J_{crit} (accounting for the enhancement in this value due to X-ray ionizations) for $T_* = 3 \times 10^4$ K (see Fig. 2): $J_{\text{LW},21} \approx 2.5 \times 10^3, 3.5 \times 10^3, 7 \times 10^3, 2.5 \times 10^4$, and 8×10^4 (from the bottom to the top). For all cases shown in this figure, the temperature evolution

is nearly isothermal at $T \sim 8000$ K once the gas density reaches $n \gtrsim 30 \text{ cm}^{-3}$.

For all cases with $J_{\text{X},21} \lesssim 10^{-2}$ in Fig. A2, the electron fraction is roughly the same at $n \simeq 10^3 \text{ cm}^{-3}$, where the bifurcation of thermal evolution occurs (vertical solid line). Thus, the corresponding values of J_{crit} does not vary very much below this X-ray intensity value. However, for $J_{\text{X},21} \gtrsim 10^{-2}$, the electron fraction remains high even at $n \simeq 10^3 \text{ cm}^{-3}$. Therefore, if $J_{\text{X},21} \gtrsim 10^{-2}$, stronger FUV intensities are required to keep the gas H₂-free—in other words, J_{crit} increases.

Finally, Fig. A3 shows the relation between the X-ray intensity and the electron fraction at $n = 10^3 \text{ cm}^{-3}$, i.e. the values on the vertical solid line of Fig. A2. These numerical results (cross symbols) are explained well by a function of $10^{-4}(1 + J_{\text{X},21}/6.7 \times 10^{-3})^{0.5}$ (dashed line). For large X-ray intensities $J_{\text{X},21} \gtrsim 10^{-2}$, x_e is roughly proportional to $J_{\text{X}}^{0.5}$; at lower intensities, X-rays do not have an appreciable effect on x_e . Previous works have shown that J_{crit} increases linearly with x_e for hard FUV spectra (e.g., Omukai 2001; Inayoshi & Omukai 2011). The above two relationships lead to the dependence of J_{crit} on J_{X} shown in this paper, and motivate the fitting formulae used in §2.3.

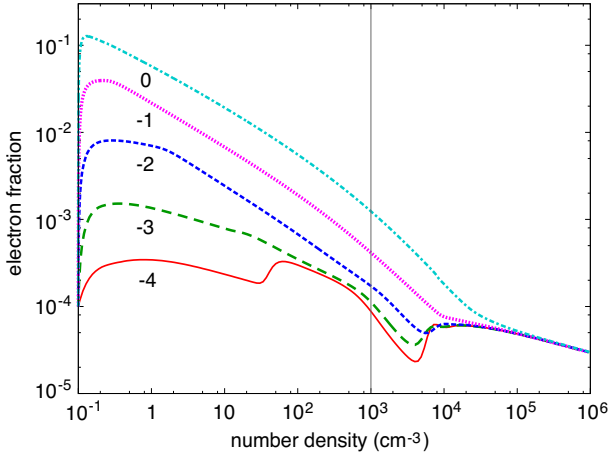


Figure A2. Evolution of the electron fraction in a collapsing cloud for $-4 \leq \log J_{X,21} \leq 0$, the values of which are denoted by numbers in the figure. For each case, the FUV intensity $J_{LW,21}$ is set slightly higher than the critical value J_{crit} for $T_* = 3 \times 10^4$ K (see Fig. 2). A colour version of this figure is available in the online version.

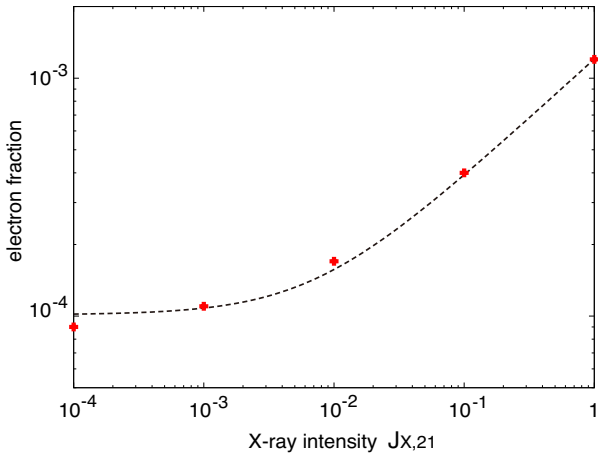


Figure A3. Relation between the X-ray intensity and the electron fraction at $n = 10^3 \text{ cm}^{-3}$ (red cross symbols), i.e. the values at the vertical solid line in Fig. A2. The dashed line is $10^{-4}(1 + J_{X,21}/6.7 \times 10^{-3})^{0.5}$. A colour version of this figure is available in the online version.